PAINLESS

D3.3– Energy neutral PHY and MAC techniques, antennas, and network level planning: phase

Grant agreement no. 812991
H2020-MSCA-ITN-2018

ITN - Innovative Training Network

D3.3– Energy neutral PHY and MAC techniques, antennas, and network level planning: phase 1

WP 3 – Research Programme

Due date of deliverable:	Month 22	
Actual submission date:	30/ 07 / 2020	
Start date of project:	01/10/2018	Duration: 48 months
Lead beneficiary for this deliverable:	5 - UMAN	
Last editor:	Igor Donevski	
Contributors:	Muhammad Haroon Tariq (ESR#2), Arzhang Shahbazi (ESR #5), Mohammad Aljraah (ESR#6), Francesco La Marca (ESR#7), Xiaoye Jing (ESR#9), Nithin Babu (ESR#10), Mahmoud Alaaldeen (ESR#14), Igor Donevski(ESR#15), Emad Alsusa	

Dissemination Level		
PU	Public	✓
PP	Restricted to other programme participants (including the Commission Services)	
RE	Restricted to a group specified by the consortium (including the Commission Services)	
CO	Confidential, only for members of the consortium (including the Commission Services)	

This document reflects only the author's view and the Agency is not responsible for any use that may be made of the information it contains.

History table

Version	Date	Released by	Comments
V1	17.07.2020	Igor Donevski, Muhammad Haroon Tariq, Arzhang Shahbazi , Mohammad Aljraah, Francesco La Marca , Xiaoye Jing, Nithin Babu, Mahmoud Alaaldeen.	Initial version
V2	17.07.2020	Emad Alsusa	
V3	28.07.2020	Igor Donevski, Muhammad Haroon Tariq, Arzhang Shahbazi , Mohammad Aljraah, Francesco La Marca , Xiaoye Jing, Nithin Babu, Mahmoud Alaaldeen.	Review and Correctoions
V4	29.07.2020	Emad Alsusa	

This document reflects only the author's view and the Agency is not responsible for any use that may be made of the information it contains.

Table of contents

This document reflects only the author's view and the Agency is not responsible for any use that may be made of the information it contains.

Key word list

Optimisation, 5G, Telecommunications, UAV, Positioning, Trajectory, mmWave, Intelligent Reflective Surfaces, Beamforming, MachineLearning, Energy autonomy, Energy harvesting.

Definitions and acronyms

Acronyms	Definitions
PAINLESS	Energy-autonomous portable access points for infrastructure-less networks
PAAs	Parasitic Antenna Arrays
RA	repeat accumulate
CVT	centroidal Voroni tessellation problem
ACNC	arithmetic sum channel decoding network coding
SBC	Smallest Bounding Circle
UE	User Equipment
VC	Voroni clustering
PNC	Physical layer network coding
LEACH	low energy adaptive clustering hierarchy
SCP	Sequential Convex Programing
KKT	Karush–Kuhn–Tucker
AAP	Aerial Access Point
AP	Access Point
DRL	Deep Reinforcement Learning
QoS	quality-of-service
ULA	uniform linear array
SER	Symbol error rate
SNR	signal-to-noise ratio
IRSs	intelligent reflecting surfaces
LOS/NLOS	Line-of-Sight /Non- Line-of-Sight
MAMP	multi active element and multiple parasitic elements

This document reflects only the author's view and the Agency is not responsible for any use that may be made of the information it contains.

SAMP	single active element and multiple parasitic elements
UAV	Unmanned Aerial Vehicle
BS	Base Station
MIMO	multiple-input and multiple-output
D-HOP	Dynamic Horizontal Opportunistic Positioning
mmWave	Milimeter wave
TIP	Telecom Infra Project
FSPL	Free Space Path Loss
D/A	digital-to-analog
A/D	analog-to-digital

This document reflects only the author's view and the Agency is not responsible for any use that may be made of the information it contains.

1. Introduction

This first (of two) phase of Energy neutral PHY and MAC techniques, antennas, and network level planning is developed as part of the energy-autonomous portable access points for infrastructure-less networks (PAINLESS) project, which has received funding from the European Union, within the H2020 Marie Skłodowska-Curie Innovative Training Networks (ITNs) framework, under the 812991 Grant Agreement.
This report corresponds to Deliverable 3.3 of Work Package 3 (WP3) Research Programme, aiming at advertising PAINLESS breakthroughs with the public. Specifically, Deliverable 3.3 revolves around describing the resource aware wireless communications models established in the first year of the project to provide a solid foundation for future developments towards energy neutrality.
Energy neutrality for portable access points is an ambitious goal that could only be reached through efficient optimization of the energy and communications resources to achieve the objective of high-performance communications. This can be done through balancing the energy consumed against the energy harvested and stored, and by developing energy-aware optimization of communications and UAV parameters (transmit power, UAV trajectory, UAV placement, etc.) to maximise energy autonomy of the Base Stations (BSs) from the power grid.
In Section 2, an overview of the general system of reference will be provided, to give the reader an idea in the context of applications of the PAINLESS findings. The final paragraph will also highlight the novelty of the work within PAINLESS.
Section 3 will give a brief description of the specific scenarios so far considered, narrowing the system to more targeted real-life applications. Sections 4 through 13 focus on providing detailed explanations on all the potential scenarios. Section 14 will conclude with a summary of the progress so far and the ambitious objectives established by PAINLESS towards building an efficient communication system.

2. System Description

The system under study cannot be described too specifically since several scenarios are considered, as exposed in Section 3. Nevertheless, a generic system can still be identified through the extended name of the project: energy-autonomous portable access points for infrastructure-less networks.
The core of this sentence is “networks”, meaning that this system’s main function is to create or expand a connectivity network, exploiting the 5G technology currently under deployment worldwide. This new standard is increasing both the quantity and the quality of data exchange, opening the path to several new mobile applications that were, until now, only possible with the use of fibre optics-based telecommunications.
The definition “infrastructure-less” is interconnected with the term “energy-autonomous”, since connectivity cables are not the only infrastructure needed by

This document reflects only the author's view and the Agency is not responsible for any use that may be made of the information it contains.

these networks: they also need a source of energy. Energy is indeed one of the focal points of the PAINLESS framework, since the 5G telecommunication standard already exists, but its exploitation is limited by energy constraints. Energy-autonomy refers to the system output during a grid-independent operation. For the purposes of PAINLESS this may be quantified by the amount of data (bits) that can be delivered per charge of the BSs, the lifetime of the grid-independent operation, and following the definition of new metrics such as energy generation vs. consumption, coverage vs. power, network performance over lifetime and operational cost vs. data rate is essential, to complement the current 5G metrics and promote energy-autonomous networks.
Energy-autonomy can be obtained by optimising three aspects, that will be extensively analysed in this report: energy harvesting, storage and balancing.
The term “portable” further specifies the system, although being a very relative term. Portability is the ability of the system to change its location, but this change of location could be a drop-and-forget application, or only partially portable and still fall within the “portable” category. Two good examples of this are represented by the BS deployable via Unmanned Aerial Vehicle (UAV) and the UAV-based Base Station coupled with a (non-portable) recharging station, both mentioned in Section 3.
In brief, the system of reference is any configuration of access points that can provide a reliable mobile network, while managing the available energy in a way that makes them independent from the grid and needing as little control and maintenance as possible.

Novelty of the work in PAINLESS

An enormous number of studies were carried out regarding 5G technology and its possible applications, but while these are getting increasingly independent by the constraints imposed by data rates, the ones imposed by energy needs remain. The novelty of PAINLESS stands in overcoming these obstacles, and doing it on three different, yet intertwined, levels:

1. converting the energy of the environment, may it be wind, sun, vibrations, or even electromagnetic fields) into electricity (energy harvesting);
2. efficiently storing the energy produced to make up for any shortages or oscillations in the energy source, as well as improving the portability (energy storage);
3. optimising the energy consumption of both the access points and their auxiliary system while achieving a specific task.

The intrinsic interdisciplinarity of such tasks makes the operation both innovative and challenging, which is why the PAINLESS consortium is composed by entities with different technical backgrounds, both from the private and the public sector. This document and the following sections focue on the third issue of the three mentioned. Here, by accounting for the communication needs for the predetermined scenario we test a variety of physical and medium access control approaches as well as testing for different antenna configurations to achieve optimal resource allocation.

This document reflects only the author's view and the Agency is not responsible for any use that may be made of the information it contains.

3. Target scenarios

Within the system described in the previous section, several more specific scenarios can be modelled. These can be categorised for portability, energy source, size, location and many other parameters, and their number is only limited by technical and economic feasibility, as well as human imagination. To discover good resource allocation many different communications technologies were considered. For convenience, the possible approaches were split into two main groups: those that do and those that do not explicitly involve the use of UAVs.

Communications-centric approaches:

In communications-centric approaches the scenario analyzed isolates itself from the complex robotic system that operates the drone, its position and trajectory. Many contemporary and state of the art techniques for addressing channel capacity and improving the conditions of the energy state are considered in this work. For further clarification, the scenario can be subdivided in three categories.

Scenarios that consider multiple transmitters and/or receivers to be mountable on the drone:

- Massive MIMO,
- Beamforming using Multi-Active and Multi-Passive Antenna Arrays.

Scenarios that include the cooperation of two separate Access Points:

- AI-enabled wireless network operation in unlicensed spectrum

Scenarios that contain Intelligent Reflecting Surfaces in the stead of using transmitting and receiving hardware:

- Wireless Mesh Backhauling Using Intelligent Reflecting Surfaces

UAV-centric approaches:

This category includes the configurations with the highest mobility with great accent on the positioning of the UAV in the three dimentinal space. In brief, the main advantages are the ability to adjust the altitude, to avoid obstacles and, consequently, to enhance the likelihood of establishing line-of-sight (LoS) communication links to ground users. Most relevant uses for UAV based BSs are the complement of existing cellular systems and the use in areas where a regular connectivity infrastructure would be too hard or expensive to build, both of which fit perfectly within the scope of PAINLESS. All this obviously comes at a cost, that is the elevated energy consumption they present, but this issue is exactly what PAINLESS is tackling. On this topic more specifically, we are interested in finding the optimal altitude and horizontal position as per sections:

- Optimal altitude for maximizing coverage probability
- Tajectory Optimization
- Altitude optimization of a standalone aerial access point
- Dynamic Horizontal Opportunistic Positioning (D-HOP) technique in Standalone Drone

This document reflects only the author's view and the Agency is not responsible for any use that may be made of the information it contains.

- Energy efficient routing architecture in a wireless and energy-autonomous network

The following sections will cover the scenarios to help towards more resource aware communications systems.

4. Massive MIMO Channel Measurements for Fixed Wireless and Smart City Applications (ESR#2)

Background:

The development of the 5th Generation networks aims at providing, among others, great capacity gains with significantly increased data rates. Millimeter-wave (mmWave) is considered a valuable asset to cater to the needs of 5G by taking advantage of wider spectrum. Several parts of the 6-300 GHz spectrum are targeted for broadband applications in the next few decades [1]. Several research efforts are being carried out to investigate the potential of mmWave communication. The suitability of mmWave frequencies is discussed in [2] for mobile communications, focusing on the propagation characteristics of mmWaves, penetration loss, doppler and multipath. The easier deployment, increased data rates and high throughput for indoor and outdoor environments is investigated in [3]. In [4]-[8], authors have mostly discussed the utilization of mmWave spectrum in access networks for 5G communications and beyond.
Path loss, penetration losses and reflection coefficients were all measured to have higher values because of the dense urban environment. In spite of all these early measurements the modeling of channels at mmWave frequencies remains an ongoing challenge. This study aims at contributing to future efforts in channel modeling at mmWave frequencies.

Measurements Plan:

We present the findings from a mmWave channel measurement campaign performed in different indoor and outdoor scenarios as part of our contribution to the mmWave Network Project Group of the Telecom Infra Project see (https://telecominfraproject.com/mmwave/). Indoor scenarios included workspace environments such as office rooms, corridors, etc. whereas, outdoor scenarios included urban and suburban environments. A set of two 802.11ad TerragraphTM Channel Sounder nodes (provided by Facebook under TIP) equipped with massive MIMO antenna arrays were used as the transmitter and the receiver for the characterization of the 60GHz mmWave channel. The measurement results include path loss, received power, input and output SNR and delay spread values for each specified beam combination. Urban, suburban and indoor environments were tested in both Line of Sight (LoS) and Non-Line of Sight (N-LoS) configurations.
The sounder nodes were used as transmitter and receiver nodes for measuring and characterizing the 60GHz mmWave channel. The nodes were provided by the Telecom Infra Project (TIP) community, along with the respective software and other peripherals. Each node has a Massive 288-element mmWave antenna array whose beam

This document reflects only the author's view and the Agency is not responsible for any use that may be made of the information it contains.

width and beam direction can be controlled by phase shifters. By choosing different modes, the beamwidth of the nodes can be varied from 2.8° to 102° and the specific beam could be scanned from -45° to 45° in either elevation or azimuth planes. Path Loss, Received Power, Input and Output SNR and Delay Spread values of the measurements is provided by the accompanied software.

Table I. consolidates different Phases/scenarios

Scenario	Tx /Rx location	Tx-Rx distance (m)	Tx/Rx height (m)	Setup
S1	AIT corridor/ AIT corridor	20	1.5	Indoor-Urban
S2	Pole/Pole	55	3.5/3.5	Outdoor-Urban
S3	Pole/Lamp-pole-I	10	2.7/2.7	Outdoor-Urban
S4	Pole/Lamp-pole-II	15	2.7/2.7	Outdoor-Urban
S5	Pole/Lamp-pole-III	22	2.7/2.7	Outdoor-Urban
S6	Pole/Lamp-pole-IV	30	2.7/2.7	Outdoor-Urban
S7	Pole/Lamp-pole-V	40	2.7/2.7	Outdoor-Urban
S8, S9	Left side of the fountain/ Right side of the fountain	24	3/3	Outdoor-Urban
S10	Ground/ First Floor	10	2/6	Outdoor-Urban
S11	Car/ Radio Tower	30-90	2/20	Outdoor-Suburban

The measurements were carried out in three different phases and in each phase, different scenarios were considered, all these scenarios are shown in the table above.

This document reflects only the author's view and the Agency is not responsible for any use that may be made of the information it contains.

(a) (b)

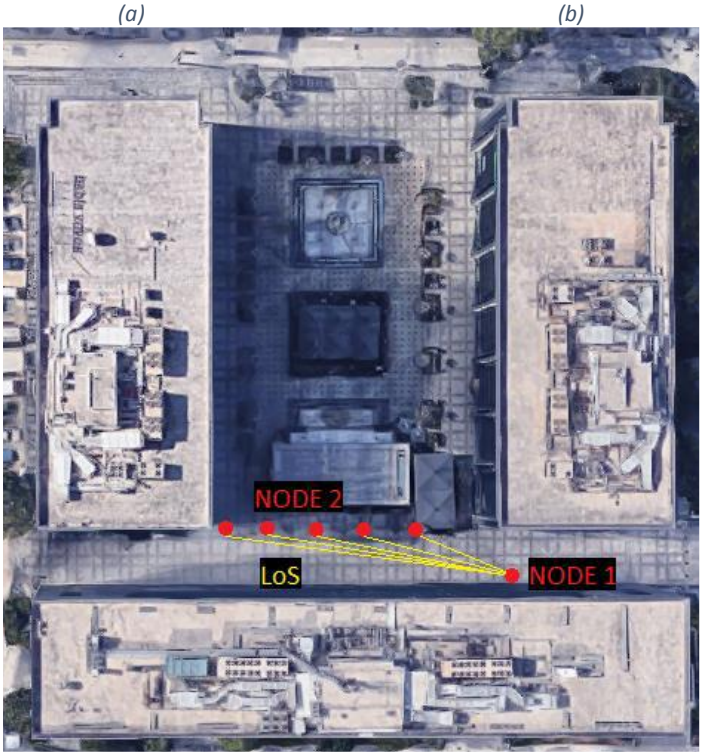

(c)

Figure 1. Measurement setup for outdoor urban and suburban environments, (a) across the water fountain outside a commercial plaza in urban environment (b) Cosmote's parking lot for suburban scenario (c) urban setup outside a commercial plaza.

This document reflects only the author's view and the Agency is not responsible for any use that may be made of the information it contains.

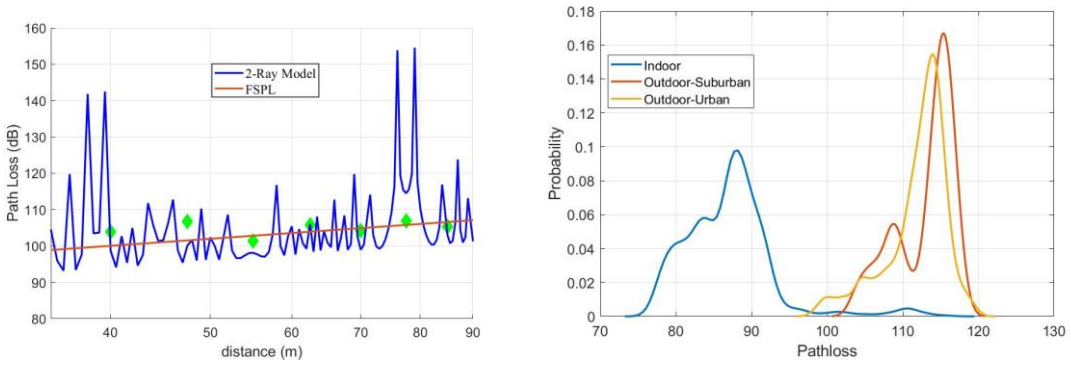

Figure 2. Measured Pathloss between Tx and Rx over different distances, compared with FSPL and 2-Ray Pathloss models (b) probability density function of Pathloss for indoor, outdoor urban and outdoor suburban scenarios.

Conclusion and Future Work:

The data collected throughout these measurement campaigns can assists the development of statistical channel models for urban environments which will be highly valuable for the development of broadband fixed wireless access using mm-wave bands in the coming years. The key takeaways from the measurements in the considered setups are summarized below.

Corporate urban plaza:

- There is a 34dB loss over the Free Space Path Loss (FSPL) due to the window attenuation (Ground-to-Floor).
- In 80% of reliable established links, the angle spread is below 10° (Pole-to-pole).
- The reflection link established shows 6.1 dB lower received power (Ground-to-Floor).
- Overall, the Rx is served reliably from all 5 positions by a fixed Tx (Poles, LoS).
- RMS delay spread can be up to 8 ns.
- Path loss from 20-60m seems better than FSPL.
- Turbulent water reflection helps the establishment of more links.

Suburban parking lot:

- Path loss from 60-90m seems to be consistent with free space transmission.
- RMS delay spread does not exceed 3.5 ns
- Thick tree foliage made it impossible to establish a link.

Office corridor:

- Path loss values approach the 2-ray model due to the density of the established links.
- CDF nicely fits the Rician distribution.

This document reflects only the author's view and the Agency is not responsible for any use that may be made of the information it contains.

5. Beamforming using Multi-Active and Multi-Passive Antenna Arrays (ESR#2)

Background:

The future demands for energy-autonomous, infrastructure-less networks have increased with the demands of high-speed data communications. This led the research community focus on an interesting topic of wireless power. The new research fascination is no wires, no contacts, no batteries, and reliable energy supply, but the challenges also emerge to provide autonomous power networks, energy limited communication devices. The research brings up new challenges and calls up the research community for integration of various involved disciplines, circuit theory, RF design, signal processing and prototyping.

The research community has widely acknowledged the multiple-input multiple-output systems as promising technology for future wireless networks. Therefore, different precoding schemes and techniques have been studied widely for energy and cost efficiency of the devices [11-13]. One of the drawbacks as compared to 4G and LTE networks, is to assign a dedicated RF chain for MIMO communication. This one RF chain includes the digital-to-analog (D/A) / analog-to-digital (A/D) converter, signal mixer and power amplifier to each antenna element in these systems, in light of the state of the art hardware implementation techniques and energy consumptions.

Parasitic Antenna Arrays (PAAs) have been used to enable new trends and paradigms for multi-antenna transmission with a single RF chain [14]. Reduction of RF chains significantly reduces energy consumption, hardware complexity, size and cost of RF circuits. It consists of one active element antenna at the center and its surrounding parasitic element antennas with adjustable reactance loads for each beam direction.

PAA design:

PAAs can be considered as prominent energy-efficient systems by reducing the power requirements of circuits as utilized by amplifiers, AC/DC converters and filters, etc. The array consists of a single active element and multiple parasitic elements (SAMP) tuned by load values also shown in Fig. 3.

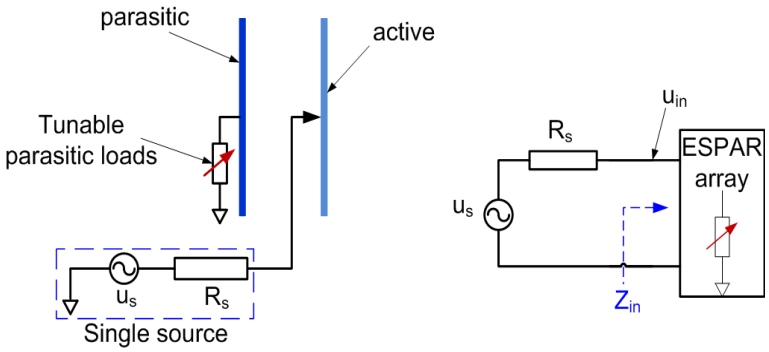

Figure 3. Equivalent circuit of single active and multiple passive antenna elements.

This document reflects only the author's view and the Agency is not responsible for any use that may be made of the information it contains.

The active element is feed through RF chain and parasitic elements receive the induced current and thus radiate. Mutual coupling is an asset here for the radiation efficiency of the array. Here coupling depends upon the distance between elements and geometry of the array structure. Desire beam direction can be achieved by tuning the load values at parasitic elements. PAAs By considering the equivalent circuit mathematical expressions can be given as;

$$\text{i} = [\boldsymbol{Z}_m + \boldsymbol{Z}_L]^{-1}\boldsymbol{v}_s \,,$$

$$\begin{bmatrix} Z_{11}+R_s & Z_{12} & \cdots & Z_{1m} \\ \vdots & \vdots & \ddots & \vdots \\ Z_{m1} & Z_{21} & \cdots Z_{mm}+x_{m-1} \end{bmatrix} \begin{bmatrix} I_0 \\ \vdots \\ I_m \end{bmatrix} = \begin{bmatrix} V_s \\ \vdots \\ 0 \end{bmatrix},$$

$$Z_{in} = Z_{11} + \sum_{m=2}^{N} Z_{1m} \frac{I_m}{I_0} \,,$$

where i is the current vector $\boldsymbol{i} = [I_1, I_2, I_3, \ldots, I_M]^T$, containing the currents on all elements of the PAA; $\boldsymbol{Z_m \epsilon\, C^{M\,X\,M}}$ is the mutual coupling matrix which is dependent on the PAAs geometry; $\boldsymbol{Z_L \epsilon\, C^{M\,X\,M}}$ is the diagonal matrix containing the complex values of the variable loads $\boldsymbol{X = \{x_1, x_2, x_3, \ldots, x_m\}}$ for each parasitic element and also the source resistance of each active element, which is usually 50 Ω. M is the total number of the elements of the array.

PAAs radiation constraints:

As per above equations, design guidelines in the form of closed form expressions and constraints are provided in [14]. The study shows that when active elements are subject to feed and load values are set to parasitic elements for desired beam directions, then it is not the case every time that array radiates. For some load values the input impedance of the structure is less then zero, resulting in absorbing energy instead of radiating.

$$R\{Z_{in}\} < 0$$

So, for PAAs to radiate the real value of input impedance must be greater than zero.

MAMP antenna arrays:

The performance of a PAA can be further enhanced for multi-antenna transmission by increasing the number of active elements, thus creating a MAMP antenna array.

This document reflects only the author's view and the Agency is not responsible for any use that may be made of the information it contains.

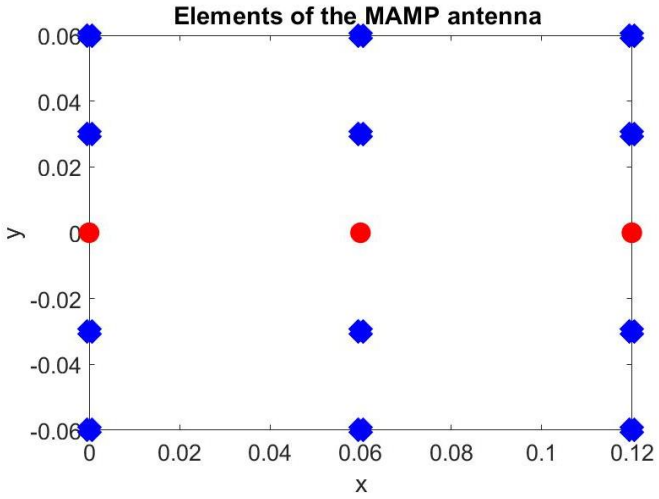

Figure 4. MAMP antenna array geometry, where dots represent the active elements and the crosses represent the parasitic elements. Spacing between active elements is 0.5λ. Spacing between parasitic elements is 0.25λ

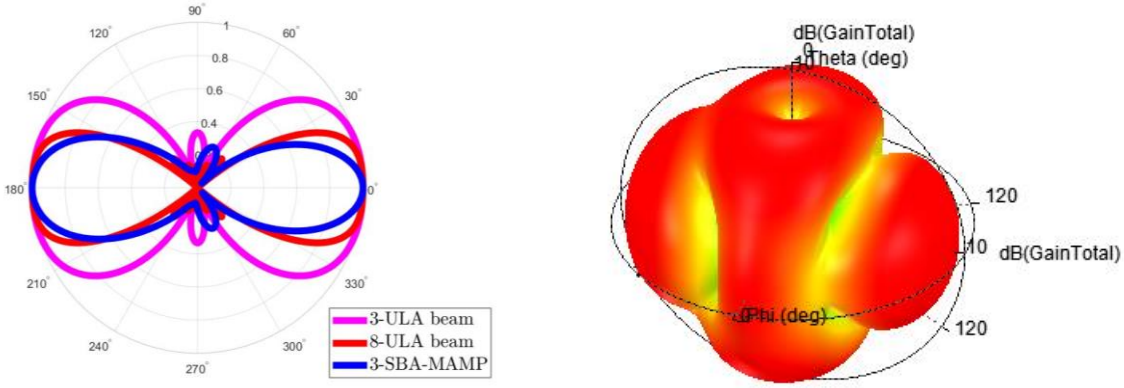

Figure 5. (a) the radiation pattern of a MAMP antenna array compared with traditional Uniform Linear Array. (b) The 3D polar plot shows the radiation pattern in all planes.

From Fig. 5, it can be seen that the radiation pattern from MAMPs is giving better results than a traditional uniform linear array (ULA). Where number of chains have reduced from 8 to 3.

This document reflects only the author's view and the Agency is not responsible for any use that may be made of the information it contains.

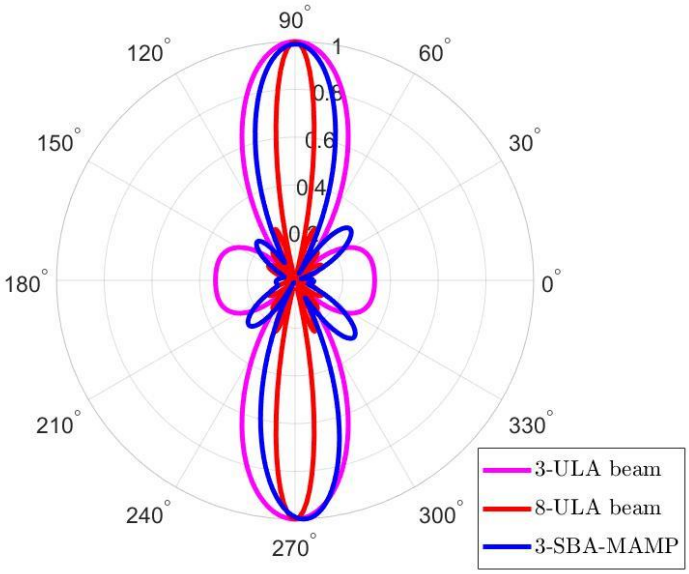

Figure 6. Radiation beam directed at φ=90° by using different load values.

From the above figures i.e. Fig. 5 and 6, energy-efficient MAMPs can be a good candidate for future energy-constrained networks with directive beamforming qualities. The future work reports the investigation and the analysis performance of the proposed MAMP array in rectenna for wireless information and power transfer. The plan is to design a highly directive and high gain antenna array that will be a good candidate for the transmission as well as for energy harvesting. To cope up with the state-of-the-art communication systems i.e., 5G, array must be designed for the mmWave frequencies to support the high data rates. This study might include designing of IRS to fulfil the needs of this proposed research. Our aim is to optimize the phases at Relay BS and IRS by minimizing the total utilized power in the system through antenna array. The study also targets the formulation and solution of new problems on how to minimize the communication power and enhancing performance of energy harvesting systems using proposed WIPT techniques.

6. Optimal altitude for maximizing coverage probability (ESR#5)

Introduction

Unmanned aerial vehicle mounted base stations have captivated significant interest from wireless system architects because of their cost effectiveness, flexibility, mobility and the ability of on-demand and fast deployment for future wireless channels [1],[2]. UAV-BSs allow terrestrial BS offloading in extremely crowded areas as well as wireless connectivity in battlefields or disaster areas. Before full use can be made of the UAV-BSs gains and many potential applications, some remaining technical challenges, such as optimal UAV-BS placement still need to be studied [3],[4].

There exist several previous studies on performance analysis of wireless networks incorporating UAVs. The horizontal and/or vertical positions of the UAVs could be opti-

This document reflects only the author's view and the Agency is not responsible for any use that may be made of the information it contains.

mized for their deployment, leading to various two-dimensional (2D) or 3D UAV placement designs [5]–[7]. In [8], the joint optimization of UAV-BS altitude and beamwidth was proposed to maximize the sum rate of multiuser communications. The authors studied three different models based on proposed fly-hover-and-communicate protocol. In [9], a novel analytical framework for the coverage probability was developed. The authors demonstrated that the LOS ball model is an excellent candidate for tractable analysis of UAV networks, while maintaining satisfactory accuracy. In [10], a study was given on energy-efficient 3D placement of a UAV-BS by adopting UAV-BS antenna tilting to minimize the total UAV-BS energy consumption. The authors converted the 3D placement problem into a 2D placement problem by obtaining the minimum altitude based on the elliptical characteristics produced by the tilted antenna.
Motivated by the above observation, to realize the full potential of UAV-enabled communication, it is essential to exploit the fully controllable UAV mobility in three-dimensional space. One of the key factors of UAV mobility is the altitude that UAV is operating in cellular networks. So far, the studies on the altitude optimization are mostly based on optimization and finding the optimal altitude numerically. However, it is crucial to conduct a mathematical approach to find a closed form expression for the optimal altitude. Thus, in this work, we propose a new analytical framework for cellular connected UAV networks, which leads to results that are more tractable than those provided by previous studies. First, we introduce a new probabilistic model for LOS and NLOS propagations in these networks, which is inspired from the 3D LOS ball model, that not only achieves high accuracy but also remains tractable. Then, with the aid of the proposed analytical framework, we evaluate the coverage probability of cellular-connected UAV which is giving service to multiple ground users in the covered region. Subsequently, we derive a novel and tractable formula for optimal altitude of cellular-connected UAV networks, which is separated to three region corresponding to three integral operations in the coverage probability expression. Based on our numerical results, the impact of the cell radius, height of the blockages, the density and the length of the blockages are investigated. In one of the scenarios, an optimal altitude is derived to maximizes the coverage probability. And in other scenarios, a lower bound on the optimal altitude is properly given. To the best of the authors' knowledge, this is the first analytical result on the optimal altitude of cellular networks which also studies the impacts of blockages on the system performance.

System Model

In this section, we describe the system model and blockage model for cellular-connected UAV networks. Consider a UAV-enabled wireless network, where a single UAV is flying in the sky to execute certain objectives. As described in the Fig. 8(a), we assumed that the UAV is at the origin and it is supplied with a directional antenna of adjustable beamwidth. Moreover, the ground users are distributed according to uniform distribution.

This document reflects only the author's view and the Agency is not responsible for any use that may be made of the information it contains.

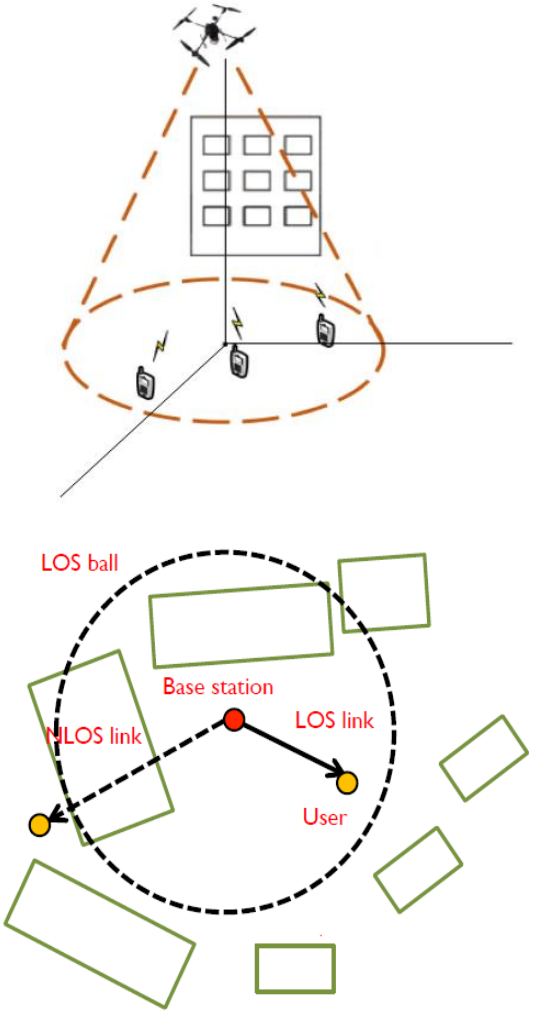

Figure 8. (a) System model with one UAV supporting ground users distributed in a disk region. (b) An illustration of LOS ball model.

In order to model the wireless link between the ground users and the UAV, the LOS and NLOS components are considered separately. Here, we present the first piece of the our analytical framework, the LOS probability in the blockage model. Based on measurement data, the LOS probability in UAV networks was given in [7, eq. (4)]. However, the proposed models are complicated and do not yield tractable analytical results and are only applicable for simulations.

The investigation of the LOS probability can be traced back to the studies of millimetre wave (mm-wave) networks, where the signals with higher frequencies are sensitive to blockages. A simple yet effective blockage model called the LOS ball was proposed in [10], where the model was shown to be an accurate approximation for the exact one. More importantly, the LOS ball model was shown to lead to a tractable analysis of mm-wave networks [10], [11]. Motivated by these studies, we refer to this model and utilise it for cellular connected UAV networks.

This document reflects only the author's view and the Agency is not responsible for any use that may be made of the information it contains.

As shown in Fig. 8(b), we define an LOS radius D_h, which represents the radius of a 3D ball. In such manner, a certain link is in LOS path, when the user is located within radius D_h, and it is zero for NLOS path. In comparison with mm-wave networks, a notable difference of the LOS ball model in cellular-connected UAV networks is that the model is not only 2D distance-dependent, but also altitude-dependent in the 3-D space. In general, the LOS radius D_h should be a monotonically increasing function of the UAV altitude H. Therefore, the higher the UAV flies, the more ground users can be in the LOS path. It should be noted that the radius of the ball depends on the environment parameters (rural or urban).

3D Distance Distribution

To analysis the coverage probability and afterwards, deriving the optimal altitude of UAV, the 3D distribution of distances are needed. Therefore, in this section, we compute the distribution of distances between the ground users and the UAV operating at the origin. In our model, we assume that N number of points are uniformly distributed in two dimensional space with respect to the density function,

$$f_r^M(x) = \frac{1}{\pi(\bar{r})^2}, \quad ||x|| \leq \bar{r}$$

Where $\bar{r}$ the radius of the covered region which is equal to $H\tan(\Theta)$. Thus, the PDF of the 2D distance r from any point in the region to the UAV (located at the region) follows the uniform distribution as follows

$$f_r(r) = \frac{2r}{(\bar{r})^2}$$

Now to find the distribution of 3D distances, we use the Jacobian transformation technique. Thus, based on this method, we will have

$$f_d(d) = \frac{\partial r}{\partial d} f_r(r)$$

Since we have

$$d = \sqrt{r^2 + H^2} \rightarrow r = \sqrt{d^2 - H^2}$$

The derivative will be equal to

$$\frac{\partial r}{\partial d} = \frac{d}{\sqrt{d^2 - H^2}}$$

and finally the 3D distribution is

This document reflects only the author's view and the Agency is not responsible for any use that may be made of the information it contains.

$$f_d(d) = \frac{d}{\sqrt{d^2 - H^2}} \times \frac{2\sqrt{d^2 - H^2}}{\bar{r}^2} = \frac{2d}{\bar{r}^2}$$

Coverage Probability Analysis and Optimal Altitude for Cellular-Connected UAV Networks

In this section, we first evaluate for coverage probability, and then derive an optimal altitude for maximizing coverage probability based on the 3D LOS ball model.

Our objective here is to evaluate the coverage probability from SNR of multiple users in the coverage area of the UAV. To achieve an accurate result, we will consider the probability of LOS and NLOS in our evaluation. So, the Coverage probability is defined as follows,

$$P = E_r \left[P\left(SNR < \tau | LOS\right) \times P_{LOS} + P\left(SNR < \tau | NLOS\right) \times P_{NLOS} \right]$$

Where the LOS/NLOS probabilities is defined,

$$P_{NLOS}(r, H, h_{BLK}) = q_{NLOS}^{[0,D)} 1\left(r \le D_{H,h_{BLK}}\right) + q_{NLOS}^{[D,\infty)} 1\left(r > D_{H,h_{BLK}}\right)$$

$$P_{LOS}(r, H, h_{BLK}) = q_{LOS}^{[0,D)} 1\left(r \le D_{H,h_{BLK}}\right) + q_{LOS}^{[D,\infty)} 1\left(r > D_{H,h_{BLK}}\right)$$

Where, $r^{\{3D\}}$ is the 3D distance of a user to the UAV, $f_{r^{\{3D\}}}$ is the PDF of 3D distances, $D_{H,h_{BLK}} = DMax\{H/h_{BLK}, 1\}$,$D = \frac{2}{\mu_{BLK}}$,h_{BLK} is the height, μ_{BLK} is the density and l_{BLK} is the length of the surrounding buildings (blockages).

Furthermore, the pathloss is defined as follows

$$l = K_s r_s^{\beta_s}$$

where r is distance from user to the UAV, K_S and β_S are the pathloss constant and exponent in the S state (LOS/NLOS), respectively. Consequently, the SNR is defined by

$$SNR = \frac{P_d H_F G_0 l^{-1}}{\Theta^2 N} = \frac{P_d G_0 H_F}{\Theta^2 N \left(K r^{\beta}\right)}$$

where P_d is the transmitted power, H_{SF} is the fading and N is the noise power.
The coverage probability, defined as the probability that the received SNR is greater than a threshold, is written as

$$P\left(SNR < \tau | LOS\right) = P\left(\frac{P_d G_0 H_F}{\Theta^2 N \left(K_{LOS} r^{\beta_{LOS}}\right)} < \tau\right)$$

This document reflects only the author's view and the Agency is not responsible for any use that may be made of the information it contains.

Now, with respect to the 3D distribution of distances from users to the UAV, we can take the integral from the coverage probability expression. Furthermore, after simplifying the equation, we find that there are three different regions corresponding to coverage probability and consequently the optimal altitude. Thus, we can state for the coverage probability, that we have three regions as,

$$P(SNR < \tau) = \begin{Bmatrix} I_1 \\ I_2 \\ I_3 \end{Bmatrix}$$

Where, I_1 is the region with only LOS users, I_2 is the region with both LOS and NLOS users and I_3 is a region with only NLOS users. Now, we need to find the optimal altitude for all three regions. For the cases of I_1 and I_3, we found that the coverage probability is a decreasing function of H, so the optimal altitude is the minimum possible altitude for these two cases. However, for the case of I_2, where we have both LOS and NLOS users in the region, we found a closed-form formula for optimal altitude,

$$H_2^*(R, D, h_{blk})$$

Simulation Results

This section focuses on verifying the analytical results derived in the previous sections by comparing them to simulation results. Moreover, we will investigate the impact of different parameters on the optimal altitude.

In Fig.9, a comparison between simulation and analytical results is provided to show that our analysis match the SNR CDF from simulations. For the set of parameters, $h_{BLK} = 100; H = 150; \Theta = 80$, we compared simulations with numerical computation for different values of D.

This document reflects only the author's view and the Agency is not responsible for any use that may be made of the information it contains.

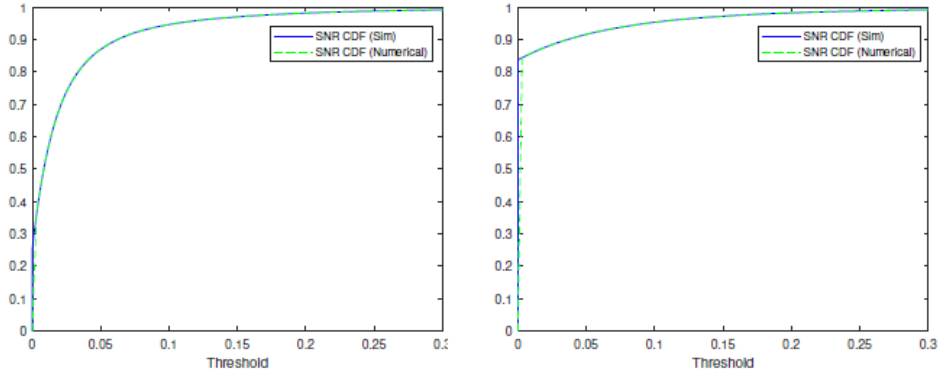

(a) SNR CDF Comparison for D = 500 (b) SNR CDF Comparison for D = 250

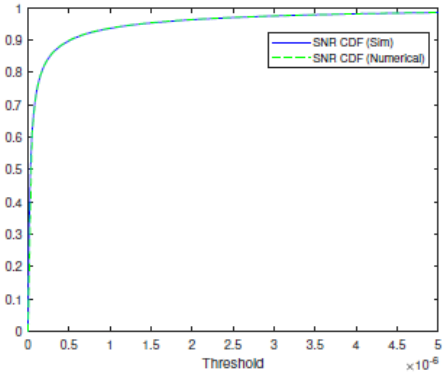

(c) SNR CDF Comparison for D = 90

Figure 9. Comparison between simulation and analytical results for SNR CDF.

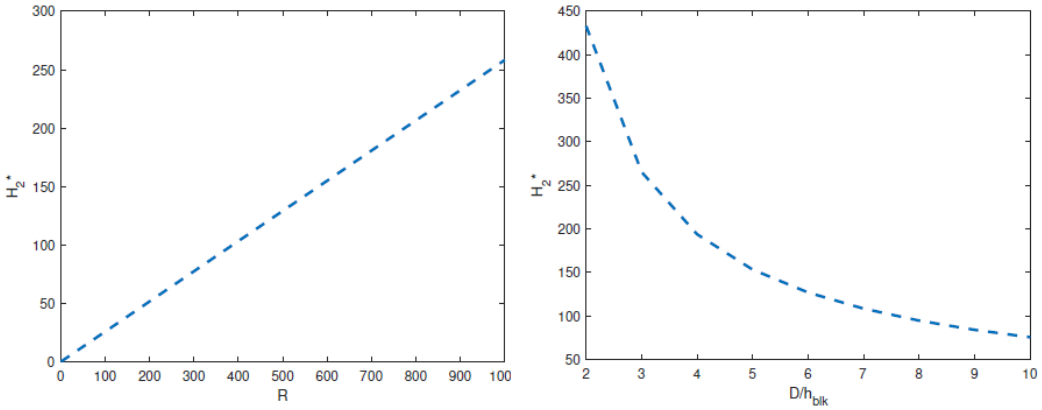

(a) Impact of R on H_2^* (b) Impact of D/h_{blk} on H_2^*

Figure 10. Figure 10. (a) Impact of the cell radius on the optimal altitude. (b) Impact of blockage height and density on the optimal altitude.

This document reflects only the author's view and the Agency is not responsible for any use that may be made of the information it contains.

Fig. 10 illustrates the impact of cell radius R, blockages height h_{BLK} and density of blockages D on the optimal altitude which was derived previously for the case of I_2. From Fig.10(a), it can be observed that by increasing the radius of the cell the optimal H increases. This means that if the UAV is scheduled to cover a larger region (covering more users), for maximizing coverage probability, the UAV altitude should be increased accordingly. From Fig.10(b), we can see that if the blockage height increases, the optimal H also increases and finally by reducing D (increasing density and length of blockages), optimal H increases. What can we conclude from is that the optimal altitude varies based on the environment that the UAV is operating. Thus, for instance, for rural areas which has lower density of blockages, the optimal altitude is lower than the urban areas which consist of skyscrapers and higher density of buildings.

Conclusion

In this work, we utilised 3D LOS ball model for coverage probability analysis and derivation of optimal altitude in cellular-connected UAV networks. We developed an analytical framework which is more tractable than existing ones. In particular, based on the our analysis for optimal altitude, we derived a closed form formula for optimal altitude which maximizes the coverage probability for one scenario, and a lower bound for two other scenarios that corresponds to the existence of LOS and NLOS users in the region. In future work, it will be interesting to study the impact of interference from nearby users on the optimal altitude and conduct a more detailed analysis of cellular-connected UAV networks in presence of interference.

7. Performance Analysis of Wireless Mesh Backhauling Using Intelligent Reflecting Surfaces (ESR#6)

As the demand for energy neutral and spectrally efficient backhauling systems for future wireless communications continues to increase, we consider the emerging technology of intelligent reflecting surfaces (IRSs) for exchanging data between basestations (BSs). IRS can be placed between communicating BSs to enhance the communication process. An IRS panel consists of multiple reconfigurable passive reflecting elements which are deployed to phase-shift multiple versions of the transmitted signal, where the values of the phase shifts are chosen to make sure that the reflected signals will be added coherently in the transmission medium; and consequently, the received signal-to-noise ratio (SNR) is considerably enhanced.

The current work considers the deployment IRSs for wireless multi-hop backhauling of multiple basestations (BSs) connected in a mesh topology. The performance of the proposed architecture is evaluated in terms of outage and symbol error probability in Rician fading channels, where closed-form expressions are derived and demonstrated to be accurate for several cases of interest. The analytical results corroborated by simulation, show that the IRS-mesh backhauling architecture has several desired features

This document reflects only the author's view and the Agency is not responsible for any use that may be made of the information it contains.

that can be exploited to overcome some of the backhauling challenges, particularly the severe attenuation at high frequencies.

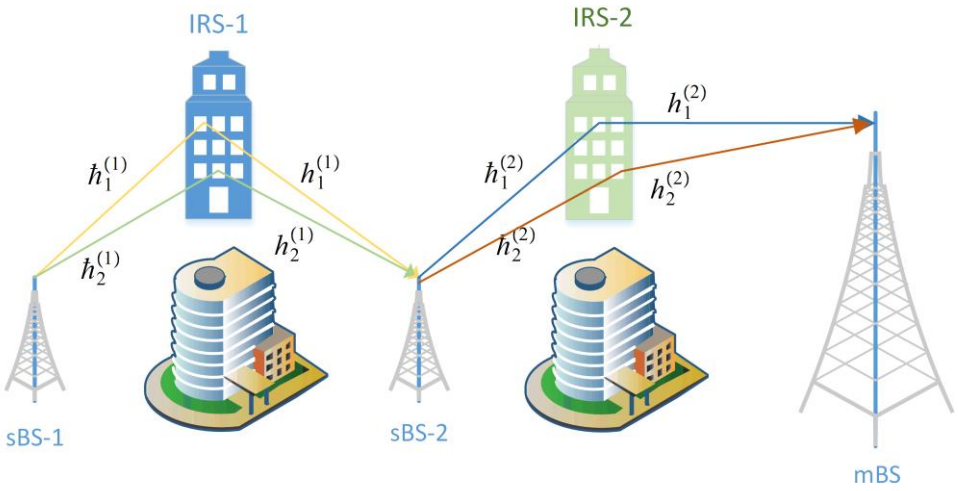

Figure 7. Example for a two-hop backhauling using IRS.

Fig. 10 presents the analytical and simulated symbol error rate (SER) using binary phase shift keying for various values of the number of reflecting elements N and the number of hops L, where the transmitted power per BS and the Rician factor K are fixed at 0 dB and 10 dB, respectively. The results show the high accuracy of the approximations used in the analysis. According to figure 10, the main difference between the IRS and a conventional multihop system in Rayleigh fading channels is that the SER degradation obtained by increasing L from 1 to 2 is about 0.35 dB at 10^{-5}, while it is about 3 dB for a conventional multihop system. Increasing the value of L beyond 4 has very limited effect on the SER.

Fig. 11 presents the analytical and simulated outage probability for various values of L and N, K = 10 dB and the minimum required SNR is γ_{th}= 5 dB. As can be noticed from figure 9, the analytical and simulation results match very well for N = 1 because outage probability is exact for this case, and for N $\geq$ 5 because the approximation accuracy improves versus N. Moreover, it can be noted that increasing N improves the outage probability significantly, and dilutes the degradation caused by increasing L. More specifically, the effect of N becomes negligible for N $\geq$ 10.

This document reflects only the author's view and the Agency is not responsible for any use that may be made of the information it contains.

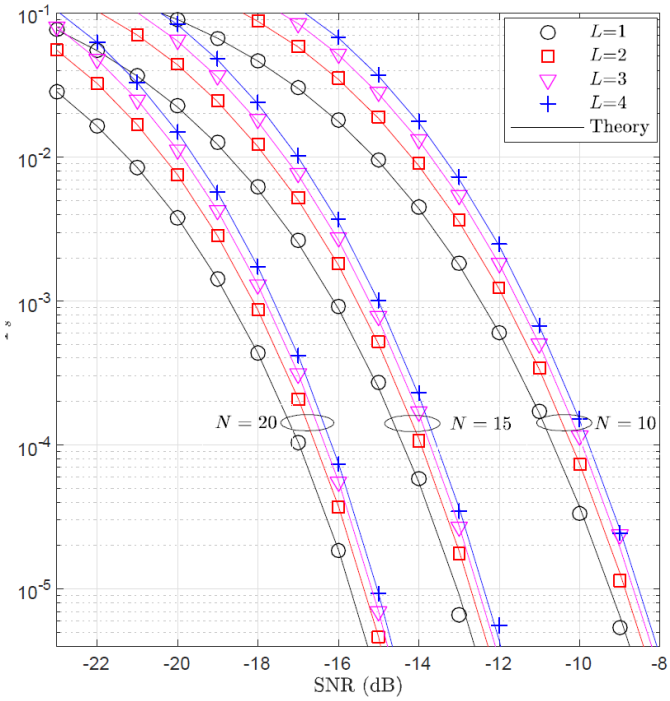

Figure 8. SER using BPSK for various values of L and N, K = 10 dB.

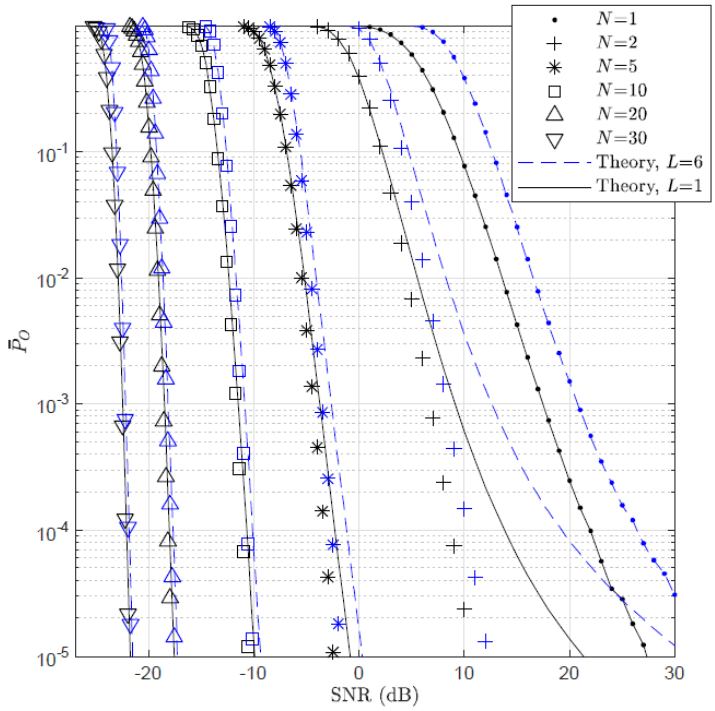

Figure 9. The outage probability for various values of N, L =1 and 6, K =10 dB and γ_{th} =5 dB.

This document reflects only the author's view and the Agency is not responsible for any use that may be made of the information it contains.

The relation to PAINLESS and next phase of the work.
As can be observed from the provided results, communications with excellent quality-of-service (QoS) can be achieved at low values of the transmission power. For example, using IRS with four elements, N = 4, provides a symbol error rate of about 10^{-5} at a signal-to-noise ratio of about 0 dB, even for a large number of hops. Therefore, deploying IRS provides an excellent candidate for energy neutral backhauling. Consequently, the next phase of this work is to consider the energy neutrality of the network by optimizing the required transmission power for a certain budget of the harvested energy. In addition, the derivations will be used for network planning by proposing a routing strategy for wireless mesh backhauling with IRS which guarantees optimizing the energy consumption of the network.

8. Intelligent wireless network operation in unlicensed spectrum (ESR#7)

The main objective of this research activity is to design a hyper intelligent wireless network operating in the unlicensed spectrum for enabling high-capacity and/or low-latency communications in future enterprise and Industry 4.0 scenarios in a cost-effective manner.

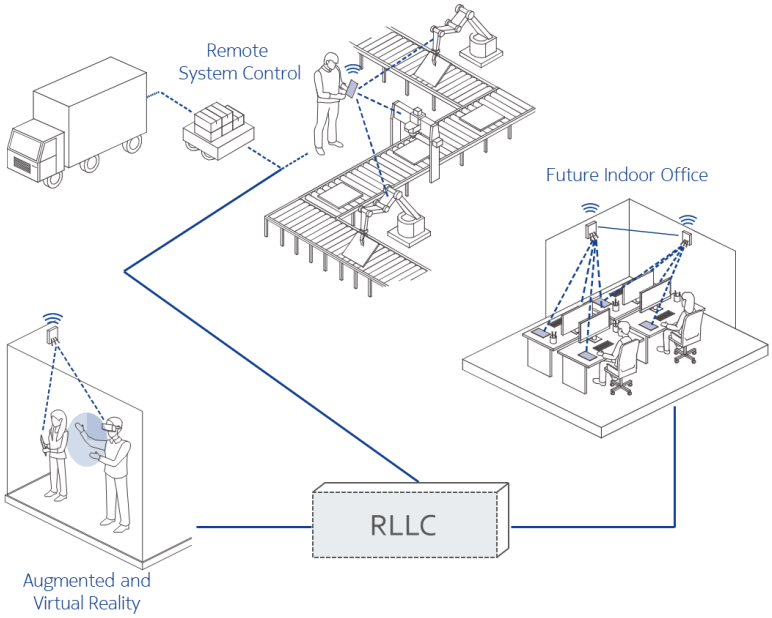

Figure 10. - Industry 4.0 Scenarios

The unlicensed spectrum presents both some opportunities, like the large amounts of available spectrum in the 2.4 GHz, 5 GHz, and 6 GHz band, but also some technical challenges such as poor performance in dense deployment scenarios due to inter-cell

This document reflects only the author's view and the Agency is not responsible for any use that may be made of the information it contains.

interference and large delays as a result of the 802.11 medium access control, based on listen-before-talk.

The next generation Wi-Fi—based on IEEE 802.11be Extremely High Throughput (EHT)— has proposed multiple new features, like 320 MHz bandwidth, 16 spatial streams, Multi-band/multi-channel aggregation and operation, Multi-Access Point (AP) Coordination to successfully support reliable low-latency communications (RLLC).

Nokia has been actively participating in the standardization process of IEEE 802.11be focusing on multi AP coordination in combination with the null-steering technique. Null steering is a technique of spatial signal processing by which antenna transmitters place nulls towards the directions of neighbouring stations (STAs). By doing so, the interference can be greatly reduced enhancing the overall network performance.

In normal operation the two Access Points (AP) take independent scheduling decisions at each Transmission Opportunity (TxOP). To optimally place the nulls towards the STAs some level of coordination is required between the APs. Given the combinatorial nature of the problem, the proposed solution that has been developed is to deploy and train a central controller (CC), through Deep Reinforcement Learning (DRL), able to take real-time optimal decisions on whom to null in each TxOP.

An example of scenario can be seen in Figure 13, where there are 2 APs, each equipped with 8 antennas, transmitting in downlink to a total of 10 STAs, each equipped with 1 antenna.

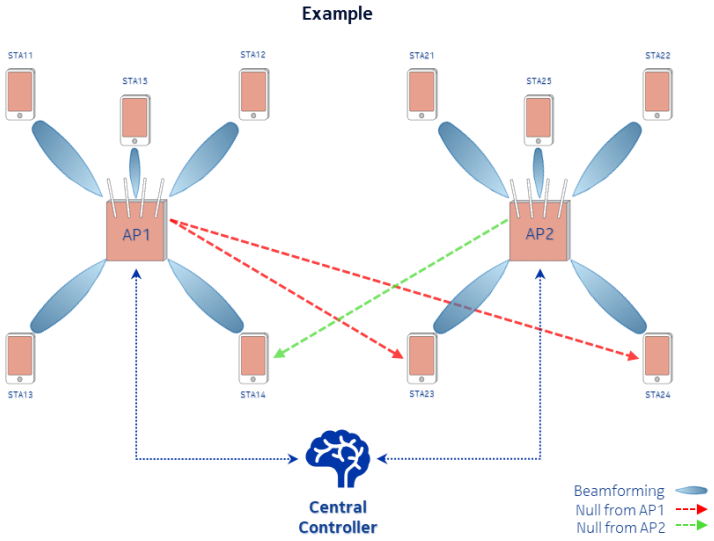

Figure 11 – Example Scenario

Figure 12 shows a comparison between the policy learned by the DRL agent and the one with no coordination between the APs. Also, it is shown the optimal policy which gives insights on how well the agent is performing with respect to the global optimum.

This document reflects only the author's view and the Agency is not responsible for any use that may be made of the information it contains.

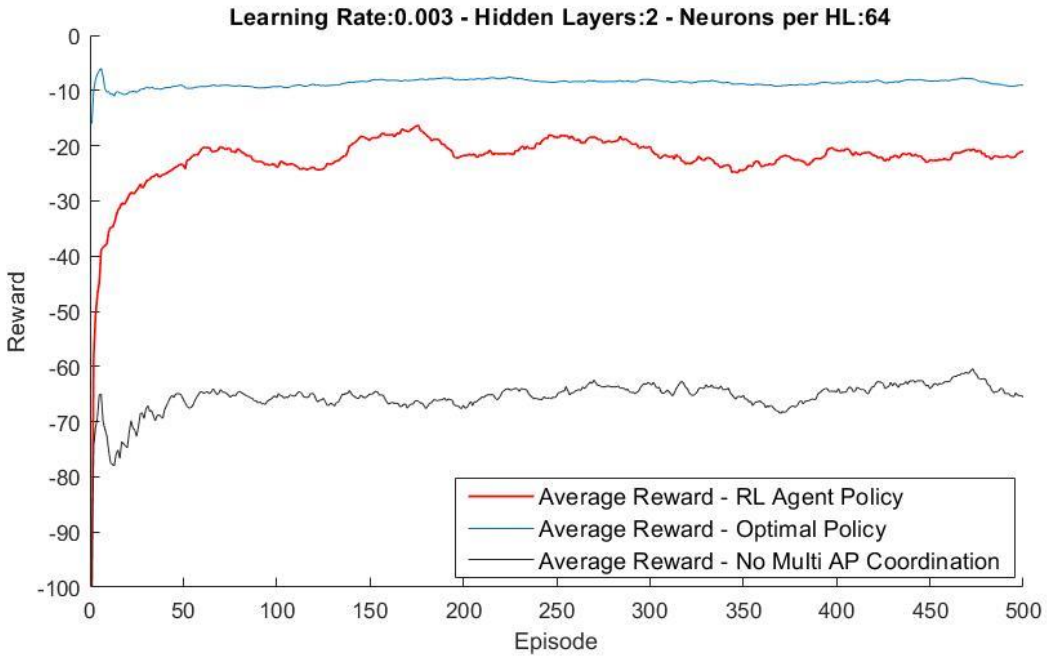

Figure 12. - Results

The reward signal used by the agent to learn how to behave in the environment is:
$R = -(N° \, Unsuccessful \, Transmissions)^2$
The agent converges within a short number of episodes, approximately 80, despite the high number of possible actions at each TxOP. Moreover, the multi AP coordination framework, combined with the null-steering technique and deep reinforcement learning, outperforms the standard Wi-Fi operation in terms of number of users successfully served by the network. This directly translates into a more reliable network where the central controller is able to intelligently manage Multi-Access Point (AP) null-steering technique and at the same time maximise the trade-off between beamforming gain and null placement.

9. Trajectory optimization (ESR#9)

Introduction
We consider a moving aerial base station which is a fixed-wing UAV. This UAV is dispatched from charging base to meet ground users' data requests. We require it to fly back to the base for recharging before exhausting its all energy.

This document reflects only the author's view and the Agency is not responsible for any use that may be made of the information it contains.

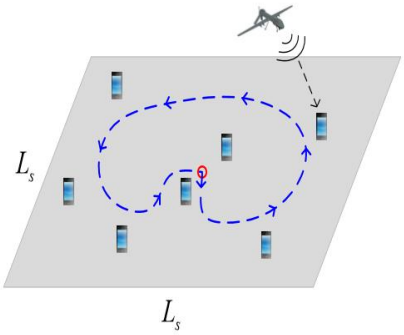

Figure 13. Scenario

First, we formulate the optimization problem. The problem is how to design the UAV trajectory to satisfy the data demand of a maximum number of ground users. Meanwhile, considering constraints on energy resources and flying status.
Secondly, about the algorithm, to tackle this formulation, we use convex optimization based on iterative algorithm. We exploit a penalty method to reformulate the optimization formulation and use block coordinate descent technique to decompose the problem into four sub-problems.

System Model

Data rate model:

$$R = TB\log_2\left(1+\frac{P_t\zeta_0}{H^2+\|\mathbf{s}-\mathbf{w}\|^2}\right) \quad (1)$$

T is time duration; B is available communication bandwidth; P_t is transmit power; ζ_0 is referenced received signal-to-noise; H is UAV altitude; $\mathbf{s}$ is UAV location; $\mathbf{w}$ is the fixed location of user.

Power model:

$$\left(c_1\|\mathbf{v}\|^3+\frac{c_2}{\|\mathbf{v}\|}\left(1+\frac{\|\mathbf{a}\|^2}{g^2}\right)\right)+P_t \quad (2)$$

$\mathbf{v}$ is UAV velocity; $\mathbf{a}$ is UAV acceleration. c_1 and c_2 are $g=9.8\,\mathrm{m/s^2}$ constant parameters related to the UAV's design, air density, etc., and represents the gravitational acceleration.

Problem formulation

$$(\mathrm{P1}):\ \underset{\{\alpha_m[n],\mathbf{s}[n],\mathbf{v}[n],\mathbf{a}[n],T[n],P_t[n],\eta_m\}}{MAX}\ \sum_{m\in\mathbf{M}}\omega_m\eta_m$$

s.t.

$$\sum_{n=1}^{N}\alpha_m[n]T[n]B\log_2\left(1+\frac{P_t[n]\zeta_0}{H^2+\|\mathbf{s}[n]-\mathbf{w}_m\|^2}\right)\geq\eta_m Q_m,\forall m \quad (3)$$

$$\eta_m\in\{0,1\},\forall m \quad (4)$$

This document reflects only the author's view and the Agency is not responsible for any use that may be made of the information it contains.

$$\alpha_m[n] \in \{0,1\}, \forall m, \forall n \tag{5}$$

$$\sum_{m=1}^{M} \alpha_m[n] \le 1, \forall n \tag{6}$$

$$\sum_{n=1}^{N} \left(c_1 \left\| v[n] \right\|^3 + \frac{c_2}{\left\| v[n] \right\|} \left(1 + \frac{\left\| a[n] \right\|^2}{G^2} \right) \right) T[n] + \sum_{n=1}^{N} P_t[n] T[n] \le E_{tot} \tag{7}$$

$$\mathbf{s}[1] = \mathbf{s}[N+1] = \mathbf{s}_0 \tag{8}$$

$$\mathbf{s}[n+1] - \mathbf{s}[n] = \mathbf{v}[n] T[n], \forall n \tag{9}$$

$$\mathbf{v}[n+1] - \mathbf{v}[n] = \mathbf{a}[n] T[n], \forall n \tag{10}$$

$$\mathbf{v}[n+1] = \mathbf{v}_0 \tag{11}$$

$$\left\| \mathbf{v}[n] \right\| \le v_{max}, \forall n \tag{12}$$

$$\left\| \mathbf{v}[n] \right\| \ge v_{min}, \forall n \tag{13}$$

$$\left\| \mathbf{a}[n] \right\| \le a_{max}, \forall n \tag{14}$$

$$T[n] > 0, \forall n \tag{15}$$

$$0 \le P_t[n] \le P_{max}, \forall n \tag{16}$$

We define a binary variable $\alpha_m[n]$ indicating the scheduling and association status of user *m* in path slot *n*. Specifically, if $\alpha_m[n]=1$, the *m*-th user is served by the UAV in path slot *n*, and otherwise $\alpha_m[n]=0$. A binary variable η_m is utilized for indicating whether the data demand of user *m* is satisfied or not. We assume that the data requested by user *m* is Q_m, $\eta_m=1$ when $R_m \ge Q_m$, and otherwise $\eta_m=0$. E_{tot} denotes the total on-board energy of the UAV; $\mathbf{s}_0$ denotes the location of the charging base; $\mathbf{v}_0$, v_{max}, v_{min} and a_{max} denote final velocity, maximum allowed speed, minimum required speed and maximum allowed acceleration of the fixed-wing UAV respectively; P_{max} is the maximum transmitting power. ω_m is a weighted factor of user m, where $\omega_m = \frac{Q_m}{Q_1 + Q_2 + \ldots + Q_M}$. Constraints (13) and (15) mean UAV cannot stay at one location, since the fixed-wing UAV cannot hover in one place. Note that, (7) guarantees that the UAV total consumed energy should be no larger than its on-board energy. According to (8), the UAV is dispatched from the charging base at the first path slot, and should fly back to the base for recharging at the end of the mission period. In addition, the UAV mobility is governed by the velocity constraints as specified in (9)-(11).

Simulation Results

This document reflects only the author's view and the Agency is not responsible for any use that may be made of the information it contains.

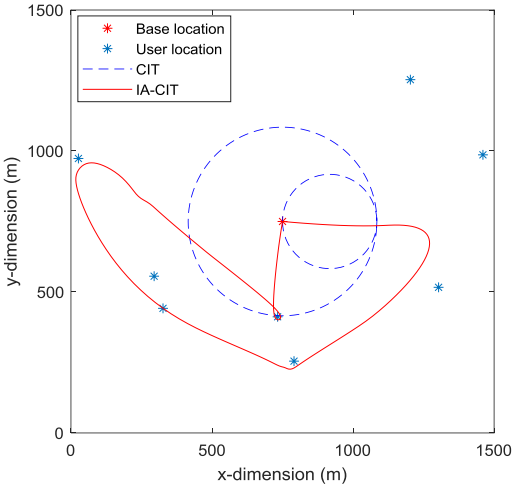

Figure 14. An Optimized trajectory

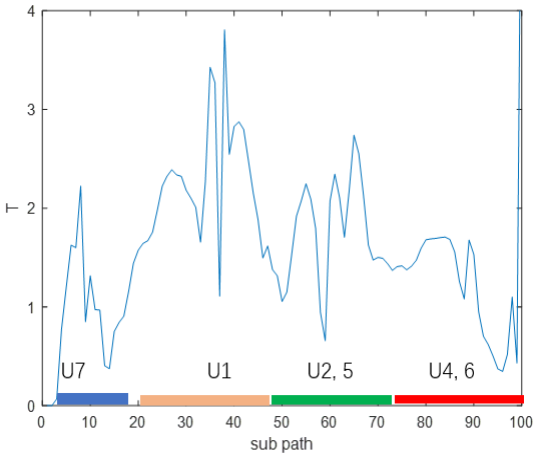

Figure 15. Time duration of UAV corresponding to the trajectory shown in Fig.15.

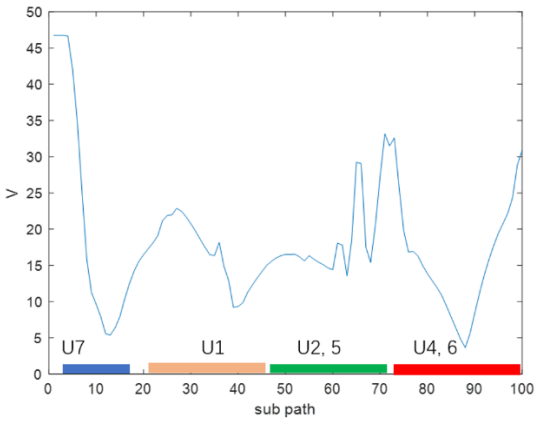

Figure 16. Speed of UAV corresponding to the trajectory shown in Fig.15.

This document reflects only the author's view and the Agency is not responsible for any use that may be made of the information it contains.

It can be seen that the UAV first flies towards the served users within a short time, then gradually spends more time flying around target users when it starts to have a good communication channel with the corresponding users and makes the communication connection with this user.

10. Altitude optimization of a standalone aerial access point (ESR#10)

State of the art

The role of uninhabited aerial access points (AAP) in the deployment of emergency networks such as deploying aerial base stations to provide reliable connectivity in disaster areas is vital. The efficiency of an aerial communication system (ACS) is highly dependent on the limited energy available at the aerial vehicle. In ACS, in addition to the communication-related energy, the aerial vehicle consumes energy during vertical climb and hovering. Most of the works in the literature only consider communication-related energy, which is suboptimal in the case of an ACS. Since the ratio of communication energy to the total energy consumed by the aerial vehicle is negligible, the results proposed in the literature are suboptimal for the global energy efficiency maximization of ACS. For instance, In [12], the authors present an analytical approach to optimize the altitude of low altitude aerial platforms to maximize the radio coverage area. The authors of [13] jointly optimize the flying altitude and the antenna beamwidth for throughput maximization. A new 3-dimensional deployment plan for the drone-base station to serve the users based on their service requirements, while minimizing the number of drones, is presented in [14]. The work in [15] proposes a new polynomial-time complex spiral mobile base station placement algorithm in UAV-UE communications. The works in [16], [17] find the optimal altitude for UAV-base stations that maximizes the number of covered users using the minimum transmit power. Our aim is to determine the optimal altitude which maximizes the GEE for an ACS considering both the energy required for communication and energy consumed by the aerial vehicle.

System Model

We consider an orthogonal multiple access downlink broadcast transmission scenario enabled by an AAP acting as a flying base station, where each user is allocated a fixed bandwidth. As shown in Fig.19, we assume a uniform distribution of N UEs in the AAP coverage area $A_u = \pi r_a^2$ such that $N = \rho_u A_u$, where ρ_u and $r_a = h_a \cot(\phi)$ represent the density of UEs and the radius of the AAP coverage area respectively, and ϕ represents the minimum elevation angle required for the line-of-sight (LoS) channel between the edge UE and the AAP [12]. the LoS channel gain between the user equipment (UE) located at a distance r_i from the center of the coverage area and the AAP is given by

$$h(r_i) = \frac{g_o}{(h_a^2 + r_i^2)} \quad (1)$$

This document reflects only the author's view and the Agency is not responsible for any use that may be made of the information it contains.

where g_o represents the channel gain at a reference distance of 1m.

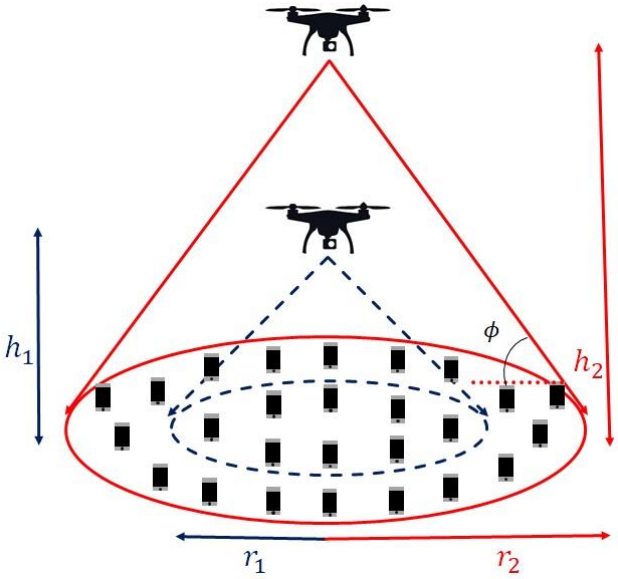

Figure 17. System Setup

Optimal vertical positioning of the aerial access point

In this Section we aim to determine the optimal altitude of the AAP which maximizes the global energy efficiency of the system. The global energy efficiency of the considered ACS is given by

$$GEE = \frac{R(h_a)}{E(h_a)} \tag{2}$$

Where $R(h_a)$ is the is the sum of the minimum number of data bits transmitted per Hz from the AAP to the N UEs in T seconds; $E(h_a) = E_a(h_a) + E_c$ is the total energy consumed by the AAP, in which E_a is the energy required for data communication and $E_a(h_a)$ is the energy consumed by the mechanical parts of the aerial vehicle given by

$$E_a(h_a) = \underbrace{\alpha_{cl} h_a + \beta_{cl}}_{\text{Climbing Energy}} + \underbrace{(\alpha_{ho} h_a + \beta_{ho})T}_{\text{Hovering Energy}} \tag{3}$$

This document reflects only the author's view and the Agency is not responsible for any use that may be made of the information it contains.

where $\alpha_{cl}, \beta_{cl}, \alpha_{ho}, \beta_{ho}$ are determined from the curve fitting performed on the measured power/energy values from the field experiments. Sum of the minimum number of data bits transmitted is derives as follows:

$$R(h_a) = T\rho_u \pi h_a^2 \cot^2\phi \log_2\left(1 + \frac{\beta}{h_a^4}\right) \quad (4)$$

where $\beta = \frac{P_t g_o \sin^2\phi}{\pi \rho_u \cot^2\phi \sigma^2}$; P_t, σ^2 are the the total data transmission power available at the AAP and the variance of the zero-mean additive white Gaussian noise at the corresponding receiver.

The objective to find the optimum altitude for the AAP, which maximizes the system's global GEE subject to minimum data rate and altitude constraints can be formulated as

(P1) $$\max_{h_a} \quad GEE$$

$$\text{Subject to} \quad h_{min} \le h_a \le h_{max} \quad (5)$$

$$W log_2\left(1 + \frac{\beta}{h_a^2(r_a^2 + h_a^2)}\right) \le R_{min} \quad (6)$$

where (5) represents the permitted AAP altitude range specified by the aviation regulatory board and R_{min} is the minimum data rate required by the UE in bits-per-second (bps). The numerator of (P1) is a non-convex function of h_a and the denominator is a convex function of h_a. The constraint (5) is a convex function and the constraint (6) is a non-convex function of h_a. Hence (P1) cannot be globally solved with convex optimization techniques. Then, we find the optimal altitude of the AAP, which maximizes the GEE of the ACS using sequential convex programming. The fundamental idea of SCP is to iteratively solve a sequence of convex approximated problems of the original non-convex problem so that the feasible solution points converge to the KKT point of the original non-convex problem [18]. The below flowchart shows the main steps of the algorithm used for solving (P1).

This document reflects only the author's view and the Agency is not responsible for any use that may be made of the information it contains.

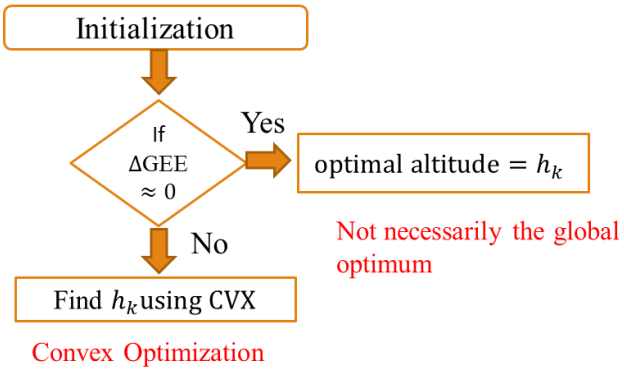

Algorithm 1. Altitude finding

In Algorithm 1, in each iteration, the convex approximated problem of the original non-convex problem is solved using the CVX toolbox[21].
The candidate solution obtained from SCP cannot be considered as the global optimum of (P1). Therefore, to obtain the global optimum of (P1), we exploit the monotonic behavior of the objective function using the monotonic fractional programming technique [19] [20]. The key idea is that the global optimum of an increasing objective function of a maximization problem lies in the outer boundary of the feasible set formed by the constraints. The below algorithm finds the global optimum of (P1) using monotonic optimization

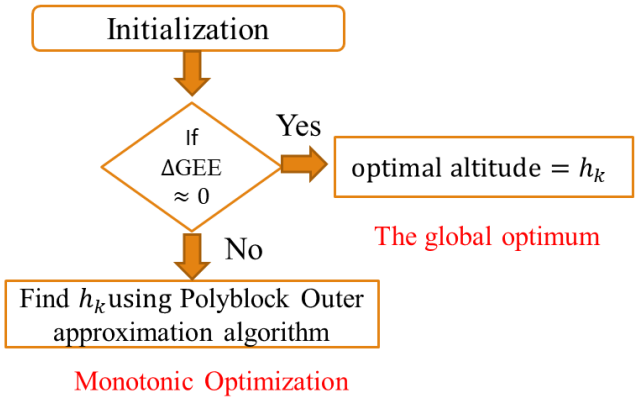

Algorithm 2. Altitude Optimization Using Monotonic optimization

In every iteration of the algorithm, the global optimium of (P1) is solved by using the polyblock outer approximation algorithm as explained in Algorithm 3 [20]. Even though the complexity of this global optimization algorithm is exponential in the number of variables, it is much lower compared to other global optimization techniques, which exhaustively search over the entire feasible set.

This document reflects only the author's view and the Agency is not responsible for any use that may be made of the information it contains.

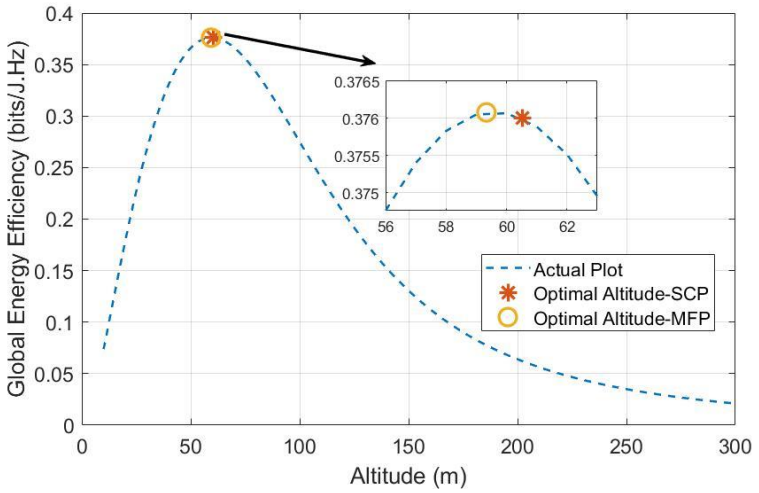

Figure 18 Optimal solutions obtained from SCP and Monotonic Optimization.

Figure 20 shows that the optimal AAP altitude obtained by the SCP is very close to the globally optimal altitude obtained from the monotonic optimization technique. Hence the global optimum of our objective can be obtained by the polynomial-time complex sequential convex optimization technique.

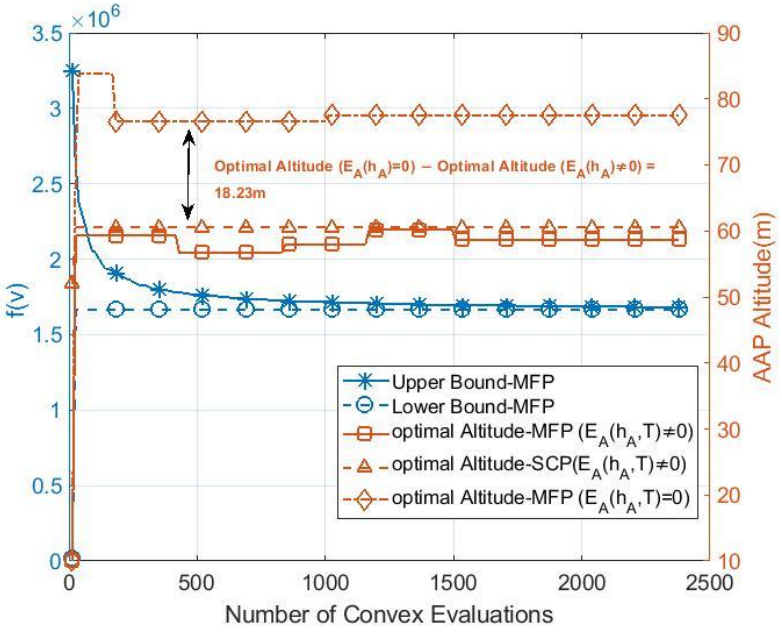

Figure 19 Convergence behavior of the PA algorithm.

Figure 21 shows the convergence behavior of the PA algorithm in the last iteration of monotonic optimization. The converging nature of upper and lower bounds of the PA algorithm guarantees the evaluation of the global optimum of GEE in a finite number of convex evaluations; with the number ofconvex evaluations much greater than that required by SCP. The optimal altitude plots of monotonic optimization and SCP says

This document reflects only the author's view and the Agency is not responsible for any use that may be made of the information it contains.

that the locally optimal altitude value obtained using SCP is equal to the globally optimal altitude obtained using MFP.

11. Energy efficient routing architecture in a wireless and energy-autonomous network (ESR#14)

In this part, the main concern is to develop an energy efficient routing architecture in a wireless and energy-autonomous network. A routing structure with both fixed and dynamic access points (APs), that have more energy than the user equipments (UEs) in the network, is proposed. This is complimented by an adaptive clustering scheme that aims at minimizing the total energy consumption of the network. We study the clustering algorithm in two scenarios. In the first scenario, the UEs slowly change their positions while in the second scenario the UEs locations frequently change so that the access points can only adapt to their statistical spatial distribution not to the actual locations. The UEs send their data first to the APs then every AP forwards the data to the remote basestation (BS). Physical layer network coding (PNC) is utilized to combine multiple received signals at the receiver coming from different synchronized transmitters and introduce the cooperative (PNC). Analysis shows that the use of cooperative PNC can lead up to 50% reduction of the transmission power when only two users cooperate. This reduction percentage can be even higher when more than two users cooperate while maintaining the same signal to noise ratio (SNR) threshold at the receiver. An extra energy saving gain is also introduced by using channel-coded cooperative PNC. This reduces the energy consumption of the network nodes and hence increasing the network longevity. The proposed routing scheme is compared against the well-known routing protocol low energy adaptive clustering hierarchy (LEACH) in two cases, the first one is direct transmission without cooperative PNC while the second is with the aid of cooperative PNC. Simulation results show a significant improvement in the energy efficiency as well as the network longevity of our routing scheme over the conventional LEACH with or without the cooperative PNC module.

System Model

This work considers a cellular network consists of a main BS, L APs, and K UEs in the whole network as shown in Fig. 22. The wireless UEs move in the cellular network within an area of $A \times A\ m^2$. Every wireless node in the network wants to transmit data to the BS that is located away from the network area. In each cell, the UEs send their data to the AP in that cell. Then, all APs aggregates the data and send them to the BS. Power control is used at the UEs such that every node can dynamically adjust its transmission power according to its transmission range. It is also assumed that all the transmit UEs are perfectly synchronized for coherent reception at the receiver. This synchronization level can be realized using the techniques discussed in previous literature.

This document reflects only the author's view and the Agency is not responsible for any use that may be made of the information it contains.

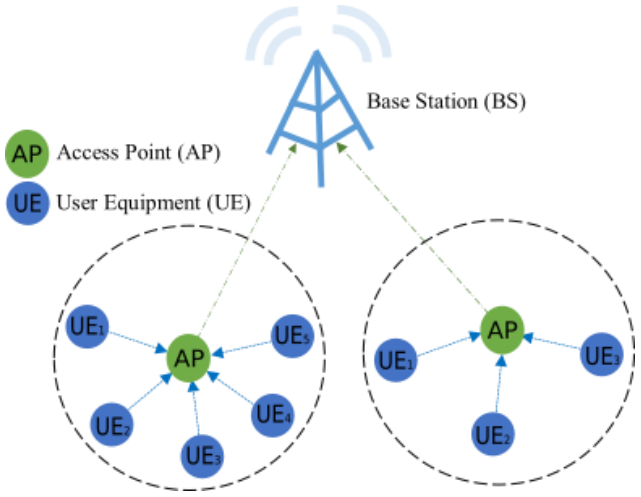

Figure 20: Network Architecture

I. Cooperative PNC

Large energy savings at each UE are achieved in each cell due to using cooperative PNC instead of point to point transmission. To illustrate the basic concept of cooperative PNC, let us consider a scenario of M UEs in a specific cell named $UE_1, UE_2, \dots, UE_M$ as shown in Fig. 22. In this scenario, UE_1 wants to transmit a packet of data symbols to the AP in the cell. These data symbols can be drawn from a QPSK modulation, but we assume here binary phase shift keying (BPSK) modulation for simplicity. When the node UE_1 transmits its data packet to the AP, the rest of the M UEs $UE_2, UE3, \dots, UE_M$ assist this transmission such that they achieve the required SNR at the AP with lower total transmitted power. While UE1 is sending its packet to the AP with power P_1, $UE2, UE3, \dots, UE_M$ transmit a known sequence of symbols X_{seq} (e.g. all zero sequence) to the AP with transmitting powers $P_2, P_3, \dots, P_M$. As long as $UE_2, UE_3, \dots, UE_M$ transmit the same known sequence X_{seq}, we can consider that their sum signal at the AP as one signal denoted as the assisting sum signal. Cooperative transmission can reduce the transmitted powers $P_1, P_2, \dots, P_M$. The synchronization between $UE_1, UE_2, \dots, UE_M$ ensures that their sum power at the AP achieves the required SNR threshold when the UEs transmit the same data symbol. However, the sum power of the received signals at the AP becomes zero when UE_1 transmit symbols that are different from the symbols of the assisting sum signal that is sent by $UE_2, UE_3, \dots, UE_M$ (i.e. symbols that are opposite in direction like 1 and -1 when BPSK is used). Consequently, the received signal form UE_1 and the assisting sum signal from $UE_2, UE_3, \dots, UE_M$ at the AP should have the same power. Since the symbols of the assisting sum signal are known at the AP, the AP can decode the data symbols of UE_1 from the combined received signal.

This document reflects only the author's view and the Agency is not responsible for any use that may be made of the information it contains.

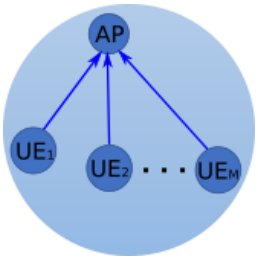

Figure 21: Cooperative PNC Scheme with M UEs

Fig. 24 shows the system performance against the average transmitted power as the number of cooperating users M increases. It shows that there is a substantial decrease in the transmitted power when more users cooperate in the PNC scheme. We used channel coded PNC in our sheme in which every UE use the repeat accumulate (RA) channel codes and the novel arithmetic sum channel decoding network coding (ACNC) at the AP in order to decode the desired XOR information.

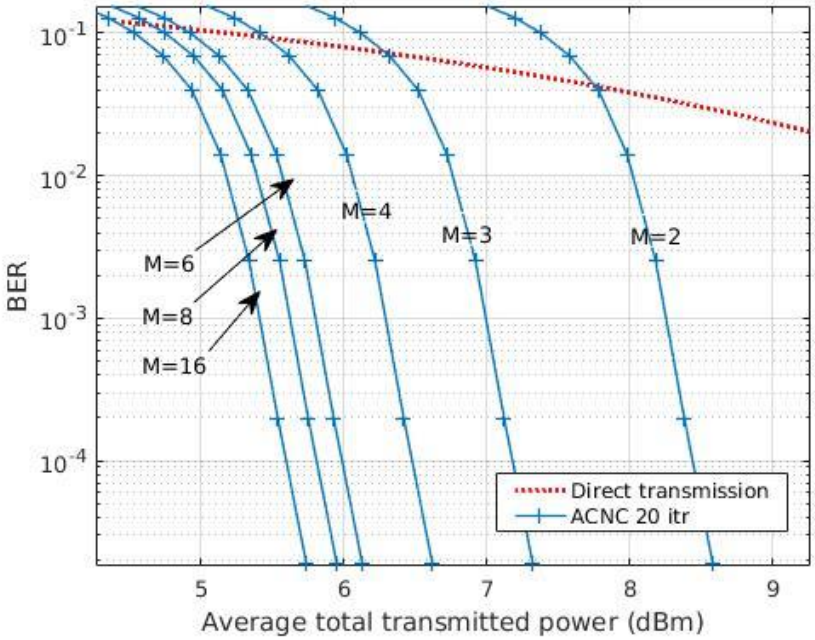

Figure 22: System performance vs average transmitted power for different M

II. Adaptive clustering:

In this section, we determine the optimum locations of the APs in the network such that the total energy consumption of the UEs is minimized. The locations of the APs are very important to be optimized as the transmission energy consumption for each packet directly relates to the Euclidean distance between the UE and an AP. We assume two scenarios for the network, the first one assumes that the UEs are static for long periods so that the APs locations can adaptively change using a drone according to the current UE locations. The second scenario assumes that the UEs randomly move

This document reflects only the author's view and the Agency is not responsible for any use that may be made of the information it contains.

in the network on fast basis that why it is not feasible to optimize the locations of the APs based on the actual UEs locations.

A. First scenario:

In this scenario, we assume that the UEs are static in each time interval and the APs locations can be adaptively optimized in each period based on the actual locations of the UEs. The optimization is based on minimizing the total energy consumption of the UEs which is transformed into a minimization of the sum of squared distances problem. This problem is called a centroidal Voroni tessellation problem (CVT) whose solution ensure that the Voroni generator point of each cluster is the centroid of the cluster, i.e. both points coincide.

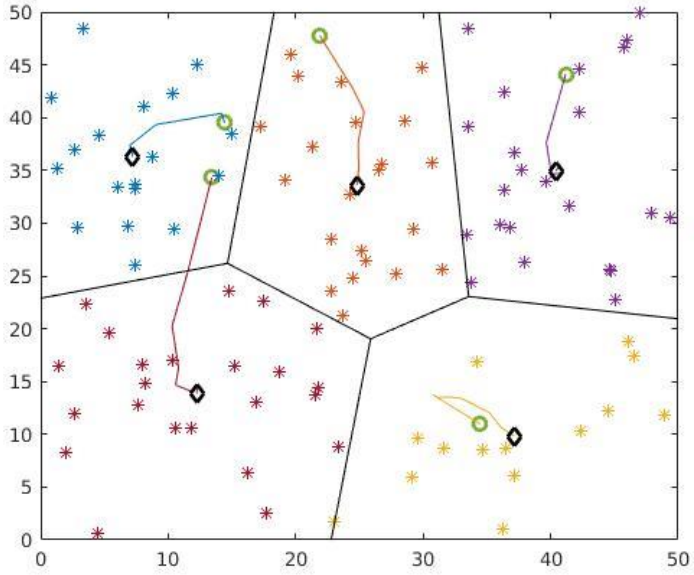

Figure 23: Scenario one, Voroni regions after optimizing the discrete CVT problem of the APs locations

B. Second scenario:

In this scenario, we assume that the UEs are randomly moving fast so that and the APs cannot follow up their changes instantaneously using drones. Hence, the optimization in this case is based on the statistical spatial distribution of the UEs in the network not the actual locations of them. Again, the optimization here aims at minimizing the average total energy consumption of the UEs when sending packets to the APs. The optimization problem here is transformed into the continuous form of a CVT problem with the statistical spatial distribution of the UEs as the density function of the CVT problem. Like the discrete case, the solution of this problem ensures that the Voroni generator point of each cluster is the mass centroid of the cluster and it is obtained using Lloyd algorithm of the continuous case. The solution of the CVT problem here depends on the density function of the spatial distribution of the UEs as well as the geometrical shape of the region which is a square in this case.

This document reflects only the author's view and the Agency is not responsible for any use that may be made of the information it contains.

III. Simulations results:

In this section, we perform simulation study in order to prove the concept of our PNC scheme and the Voroni clustering (VC) in reducing the energy consumption of the UEs as well as increasing the network longevity. The network in our simulations has 100 nodes and we have 5 access points. Assuming that the overall energy stored in the network is 100 Joules distributed among both the APs and the UEs. Based on some energy calculations, we split the 100 Joules among the access points according to the required energy at each access point to serve all the UEs in its cluster till they completely die. We compare our scheme here with LEACH as a benchmark while using the same amount of total energy of 100 Joules for a fair comparison. Fig. 26 compares the system lifetime for the first scenario when using the PNC or not as well as when using random clustering (RC), i.e. using any random locations for the APs, or using the Voroni clustering (VC) discussed in the previous sections.

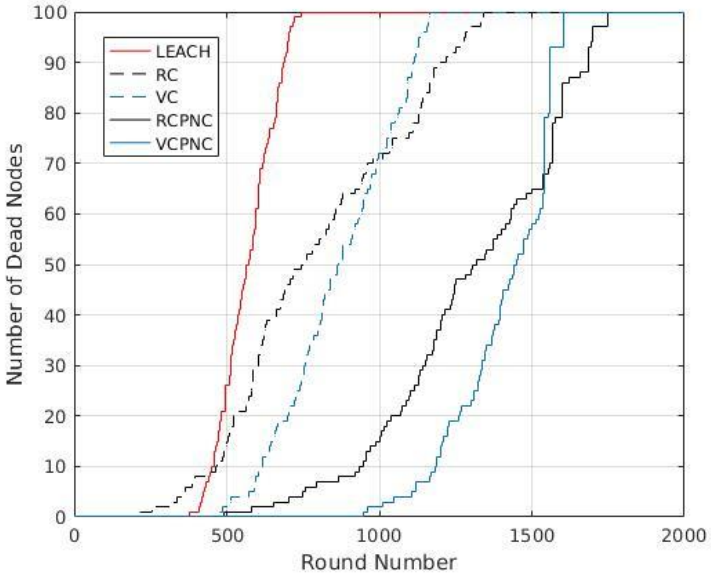

Figure 24: Scenario one, Comparison between schemes for system lifetime

Fig. 27, compares the system lifetime in the second scenario when using the PNC scheme with random clustering (RCPNC) or with Voroni clustering (VCPNC). Also, it shows that the performance significantly decreases when removing the PNC scheme from the system which concludes that it has large energy saving gains in the system.

This document reflects only the author's view and the Agency is not responsible for any use that may be made of the information it contains.

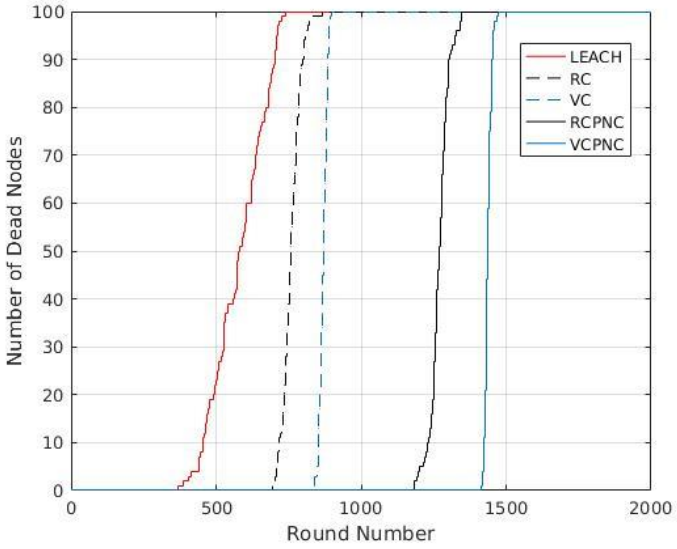

Figure 25: Scenario two, Comparison between schemes for system lifetime

12. Choosing an altitude and Dynamic Horizontal Opportunistic Positioning (D-HOP) technique in Standalone Drone Mounted Small Cells (ESR#15)

The flying UAVs are considered useful as drone mounted access points that provide or improve localized communication quality. In accord, the need for airborne base stations has been accentuated in the last five years, as it can be noticed from the overabundance in scientific and standardization activity. The concept has been identified as useful in diverse use cases: disaster recovery missions, failures of the main infrastructure, coverage assistance for traffic surges or sinks for Internet of Things (IoT) devices.
This part of the work is centered on investigating the combination and compatibility of: using a directional transmitter, the impact of the antenna's efficiency in fitting the beamwidth requirements, and most importantly, its impact on D-HOP improvements for active users. Within this work, we test the performance of three D-HOP techniques, and discuss on choosing the most adequate one for Standalone DSCs. As such, the antenna efficiency has a central role to D-HOP usefulness.

This is the first work to investigate the combination and compatibility of: using a directional transmitter, the impact of the antenna's efficiency in fitting the beamwidth requirements, and most importantly, its impact on D-HOP improvements for active users. Within this work, we test the performance of three D-HOP techniques, and discuss on choosing the most adequate one for Standalone DSCs. As such, the antenna efficiency has a central role to D-HOP usefulness. Many works although considering directional antennas, do not account for the impact of the efficiency of the transmitter, are

This document reflects only the author's view and the Agency is not responsible for any use that may be made of the information it contains.

mainly concerned with 3D placement of the drone and omit analysis on the benefits of different D-HOPs. Other, are mainly concerned with the location of the drone, assume that they do operate in a non-standalone manner, and omit the impact of directional transmitters altogether. With this, we hope to introduce the reader to the potential benefits and implementation complexities that concern deployment of D-HOP enabled standalone DSCs.

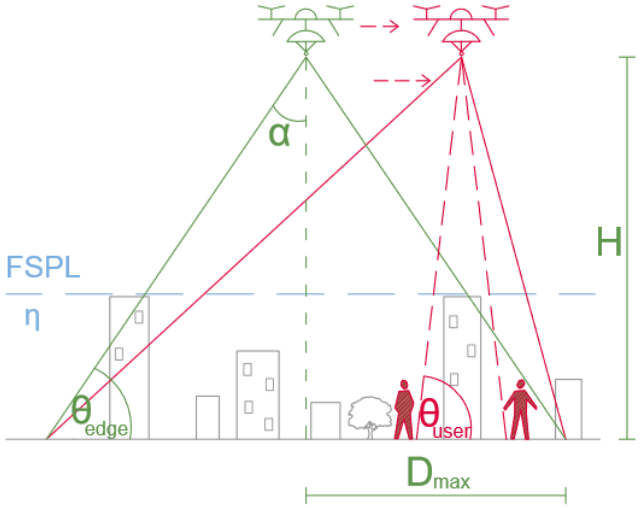

Figure 26 Example scenario of a D-HOP being implemented (Red) wit hregards to a classic reference static drone (Green)

System Model

We define the total path loss as a combination of Free Space Path Loss (FSPL) and the expected shadowing coefficient for each of the propagation groups and. These values represent the means of the normally distributed excessive path loss, that is induced due to the large features of the topology in LoS and NLoS, respectively. Assuming a directional antenna with directivity measure D_t is mounted on the drone, we can define the average path loss as:

$$10\log(\Lambda) = \frac{\eta_{\text{LoS}} - \eta_{\text{NLoS}}}{1 + a\exp(-b[\theta_{\text{user}} - a])} + 20\log\left(\frac{D_{\max}}{\cos\left(\theta_{\text{user}}\frac{\pi}{180}\right)}\right) - E_r 10\log\left(\frac{2}{1-\sin\left(\theta_{\text{edge}}\frac{\pi}{180}\right)}\right) + 20\log\left(\frac{f4\pi}{c}\right) + \eta_{\text{NLoS}}$$

Finding the first derivative of the radius cell radius Dmax, the above equation as a function of the elevation angle theta:

This document reflects only the author's view and the Agency is not responsible for any use that may be made of the information it contains.

$$0 = \frac{\pi \tan\left(\theta \frac{\pi}{180}\right)}{9\log(10)} + \frac{a\,bA\exp(-b(\theta - a))}{a\exp(-b(\theta - a) + 1)^2} - E_r \frac{\pi \cos\left(\theta \frac{\pi}{180}\right)}{18\log(10)(1 - \sin\left(\theta \frac{\pi}{180}\right))}$$

Plotting the optimal theta as a function of Er we get:

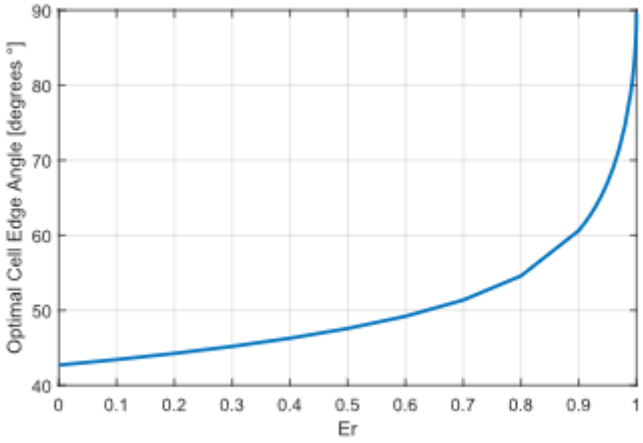

Figure 27 The impacct of antenna efficiency on the optimal deployment altitude for a reference drone

If we want to measure the increase in average rate difference for users in the cell we use:

$$R_i = \log_2(1 + \frac{\Lambda(\kappa_i = 1, D_{\max})}{\Lambda(\kappa_i, D_{\max})}) = \log_2(1 + 10^{\frac{G_{\text{pos}}(\kappa_i = 1) - G_{\text{pos}}(\kappa_i)}{10}})$$

We strive to measure the performance of three different positioning techniques and evaluate how they redistribute the users inside the cell.

Smallest Bounding Circle (SBC)

One approach that carries great geometric significance, is to set the DSC location in the center of the minimum bounding circle of all active users, which is the smallest circle that contains all points inside. With this, the goal is to maximize the fairness of the dynamic system by minimizing the maximum possible distance to all users. The minimum bounding circle is a well-known computational geometry problem falling under the umbrella of facility location, or the 1-center problem.

Maximum Aggregated Rate (MAR)

The second position of geometric significance is where drone placement would achieve minimal total distance to all active users, the centroid of all points. Although the SBC is a universal fairness maximization approach, the centroid is not, and we substitute it for

This document reflects only the author's view and the Agency is not responsible for any use that may be made of the information it contains.

a more adequate performance parameter. In its stead we use the aggregate rate improvement, as:

$$\max_{x_d, y_d} \sum_{i=0}^{N} R_i$$

Center-Most Point (CMP)

Finally, limitations regarding the mobility of the UAV need to be considered as it cannot instantaneously relocate on every position with every shift in user behaviour. This requires inspecting a more travel distance conservative repositioning technique. In favor of this, we create a repositioning algorithm that puts the drone either at maximum gain, or maximum fairness, depending on which of both points is the Centermost Point. This is done knowing that if averaged over an infinite number of users and timeslots, the optimal position of the drone is in the very center.

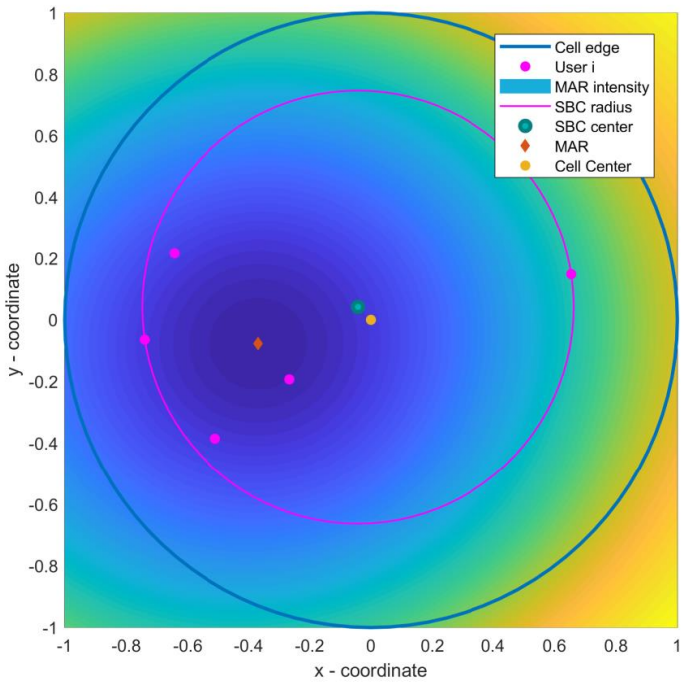

Figure 28 Illustration of the implemented D-HOP techniques

For testing we consider a snapshot based, simplistic and replicable testing scenario where the positioning of the UE occurs in timeslots, and each timeslot has no correlation to the previous one. No assumptions are done with user mobility in mind, and each user can be uniformly located within the cell's limits. We test the system under the Urban scenario conditions for a carrier of, f=2GHz for four different densities of univormly distributed users.

This document reflects only the author's view and the Agency is not responsible for any use that may be made of the information it contains.

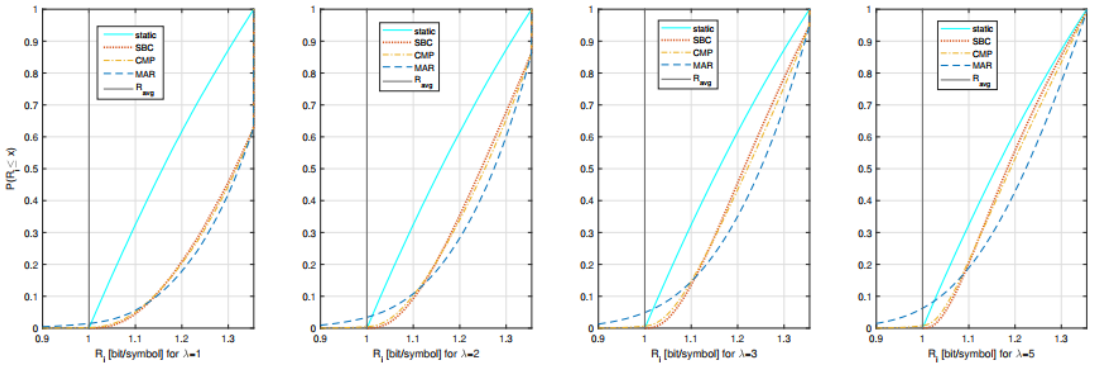

Figure 29 Results for the achieved rates for the D-HOP enabled drone with 4 different user densities

This work investigates the concept of DSCs and accounts for exploiting all its advantages. We note the importance of knowing the efficiency of the available antenna equipment as it directly influences the optimal geometry of the model. We then quantify its impact over the dynamic repositioning gains and conclude that the gains achieved from repositioning are mainly beneficial when using small antennas. For the tested urban scenario, we achieve per user average rate improvements of up to 20-35% in low-user density scenarios, or 3% - 5% in dense scenarios. Which for our model is extremely well considering we assume balanced and uniform user positions with standalone and constant coverage over the whole area.

13. Conclusions

In this first phase of the "Energy neutral PHY and MAC techniques, antennas, and network level planning" within the PAINLESS project we reached a good understanding of several concepts when working on the Physical (PHY), Medium Access Control (MAC) or antenna design. Firstly, to achieve the claim of energy neutrality we need to assume an energy source that can provide the system with an appropriate amount of energy. Secondly, engineering an efficient communication system requires energy aware design. Additionally, an important aspect of analysis is to adapt the design of the autonomous portable access point according to its purpose. As such analyzing the trajectory and position of the potential system is of utmost importance. And to know the optimal mode of operation, a well-defined set of goals needs to be defined.

The only way to accomplish such an ambitious plan of designing energy-autonomous portable access points for infrastructure-less networks is to address all these three issues at the same time, seeking the best possible solution for each. As of now weight awareness is only marginal and needs to be taken into account upon merging this work with the energy modelling part of the project. Furthermore, each solution must be compatible with the others, making cooperation crucial. In fact, a good connection among all these research fields will trigger the multiplication factor for which the outcome of a work of ensemble is greater than the sum of each single piece of research.

This document reflects only the author's view and the Agency is not responsible for any use that may be made of the information it contains.

This is true for the energy modelling and optimisation sub-group and for the whole PAINLESS project as well.
The future plan of this part of the project is to reach communication design that is able to fulfil the energy neutrality task laid down as a project motivation. This can be achieved by making a robust proof of concept that shows the possibility of a potential implementation of a device that offers drone based autonomous communications that enable a more modular and flexible, infrastructure-less grid. The main objective within this project would be to answer the practability and optimality of different communications techniques potentially useful for PAINLESS project by month 40, when phase 2 of the energy modelling and optimization is due. With this the final efforts will be focused on testing a proof-of-concept that would provide an evaluation of the actual potential of the proposed solutions, both technically and economically speaking.

References

1. Ming Xiao, Shahid Mumtaz, Yongming Huang, Linglong Dai, Yonghui Li, Michail Matthaiou, George K. Karagiannidis, Emil Björnson Kai Yang, Chih-Lin I, Amitabha Ghosh, “Millimeter Wave Communications for Future Mobile Networks”, IEEE Journal on Selected Areas in Communications, Vol. 35, No. 9, pp 1909-1935, September 2017.
2. Zhouyue Pi, Farooq Khan, Samsung Electronics, “An Introduction to Millimeter-Wave Mobile Broadband Systems”, IEEE Communications Magazine, pp 101-107, June 2011.
3. Jia Shi, Lu Lv , Qiang Ni ,Haris Pervaiz, Claudio Paoloni, “Modeling and Analysis of Point-to-Multipoint Millimeter Wave Backhaul Networks”, IEEE Transactions on Wireless Communications, Vol. 18, NO. 1, pp. 268-285, January 2019.
4. T. S. Rappaport et al., “Millimeter wave mobile communications for 5G cellular: It will work!” IEEE Access, vol. 1, pp. 335–349, May 2013.
5. S. Rangan, T. S. Rappaport, and E. Erkip, “Millimeter-wave cellular wireless networks: Potentials and challenges,” Proc. IEEE, vol. 102, no. 3, pp. 366–385, Mar. 2014.
6. T. Bai and R. W. Heath, Jr., “Coverage and rate analysis for millimeterwave cellular networks,” IEEE Transactions on Wireless Communications, vol. 14, no. 2, pp. 1100–1114, Feb. 2015.
7. C. Wang and H.-M. Wang, “Physical layer security in millimeter wave cellular networks,” IEEE Transactions on Wireless Communications, vol. 15, no. 8, pp. 5569–5585, August 2016.
8. Y. Ju, H. M. Wang, T. X. Zheng, and Q. Yin, “Secure transmissions in millimeter wave systems,” IEEE Transactions on Communications, Vol. 65, no. 5, pp. 2114–2127, May 2017.

This document reflects only the author's view and the Agency is not responsible for any use that may be made of the information it contains.

9. Md Maruf Ahamed, Saleh Faruque, “Broadband Communications Networks - Recent Advances and Lessons from Practice”, published by IntechOpen, chapter 4, pp 44-58, 2018.
10. Theodore S. Rappaport, Shu Sun, Rimma Mayzusi, Hang Zhao, Yaniv Azar, Kevin Wang, George N. Wong, Jocelyn K. Schulz, Mathew Samim, Felix Guiterrz, “Millimeter Wave Mobile Communications for 5G Cellular: It Will Work!”, IEEE Access, Volume 1, pp 335-349, May 10, 2013.
11. N. Babu, K. Ntougias, C. B. Papadias, and P. Popovski, “Energy efficient altitude optimization of an aerial access point,” in IEEE 31st PIMRC’20 - Workshop on UAV Communications for 5G and Beyond (PIMRC’20 WS - UAV 5G & Beyond), London, United Kingdom (Great Britain), Aug. 2020.
12. A. Al-Hourani, S. Kandeepan, and S. Lardner, “Optimal lap altitude for maximum coverage,” IEEE Wireless Communications Letters, vol. 3, no. 6, pp. 569–572, Dec 2014.
13. H. He, S. Zhang, Y. Zeng, and R. Zhang, “Joint altitude and beamwidth optimization for uav-enabled multiuser communications,” IEEE Communications Letters, vol. 22, no. 2, pp. 344–347, Feb 2018.
14. E. Kalantari, H. Yanikomeroglu, and A. Yongacoglu, “On the number and 3d placement of drone base stations in wireless cellular networks,” in 2016 IEEE 84th Vehicular Technology Conference (VTC-Fall). IEEE, 2016, pp. 1–6.
15. J. Lyu, Y. Zeng, R. Zhang, and T. J. Lim, “Placement optimization of uav-mounted mobile base stations,” IEEE Communications Letters, vol. 21, no. 3, pp. 604–607, 2016.
16. M. Alzenad, A. El-Keyi, F. Lagum, and H. Yanikomeroglu, “3-d placement of an unmanned aerial vehicle base station (uav-bs) for energyefficient maximal coverage,” IEEE Wireless Communications Letters, vol. 6, no. 4, pp. 434–437, 2017.
17. M. Mozaffari, W. Saad, M. Bennis, and M. Debbah, “Drone small cells in the clouds: Design, deployment and performance analysis,” in 2015 IEEE Global Communications Conference (GLOBECOM). IEEE, 2015,pp. 1–6.
18. B. R. Marks and G. P. Wright, “Technical note-a general inner approximation algorithm for nonconvex mathematical programs,” Oper. Res., vol. 26, no. 4, pp. 681–683, Aug. 1978. [Online].
19. A. Zappone, E. Bj¨ornson, L. Sanguinetti, and E. Jorswieck, “Globally optimal energy-efficient power control and receiver design in wireless networks,” IEEE Transactions on Signal Processing, vol. 65, no. 11, pp. 2844–2859, June 2017.
20. Y. J. A. Zhang, L. Qian, and J. Huang, “Monotonic optimization in communication and networking systems,” Found. Trends Netw., vol. 7, no. 1, pp. 1–75, Oct. 2013. [Online]. Available: http://dx.doi.org/10.1561/1300000038
21. M. Grant and S. Boyd, “CVX: Matlab software for disciplined convex programming, version 2.1,” http://cvxr.com/cvx, Mar. 2014.

This document reflects only the author's view and the Agency is not responsible for any use that may be made of the information it contains.

22. A. Fotouhi et al., "Survey on UAV Cellular Communications: Practical Aspects, Standardization Advancements, Regulation, and Security Challenges," in IEEE Communications Surveys \& Tutorials 2019.
23. M. Mozaffari, W. Saad, M. Bennis, Y. Nam and M. Debbah, "A Tutorial on UAVs for Wireless Networks: Applications, Challenges, and Open Problems," in IEEE Communications Surveys \& Tutorials, vol. 21, no. 3, pp. 2334-2360, thirdquarter 2019.
24. A. Fotouhi, M. Ding and M. Hassan, "Dynamic Base Station Repositioning to Improve Performance of Drone Small Cells," 2016 IEEE Globecom Workshops (GC Wkshps), Washington, DC, 2016, pp. 1-6.
25. M. Mozaffari, W. Saad, M. Bennis and M. Debbah, "Mobile Unmanned Aerial Vehicles (UAVs) for Energy-Efficient Internet of Things Communications," in IEEE Transactions on Wireless Communications, vol. 16, no. 11, pp. 7574-7589, Nov. 2017.
26. A. Al-Hourani, S. Kandeepan and A. Jamalipour, "Modeling air-to-ground path loss for low altitude platforms in urban environments," 2014 IEEE Global Communications Conference, Austin, TX, 2014, pp. 2898-2904.
27. B. Galkin, J. Kibiłda and L. A. DaSilva, "A Stochastic Model for UAV Networks Positioned Above Demand Hotspots in Urban Environments," in IEEE Transactions on Vehicular Technology, vol. 68, no. 7, pp. 6985-6996, July 2019.
28. M. M. Azari, F. Rosas and S. Pollin, "Cellular Connectivity for UAVs: Network Modeling, Performance Analysis, and Design Guidelines," in IEEE Transactions on Wireless Communications, vol. 18, no. 7, pp. 3366-3381, July 2019.
29. W. L. Stutzman, "Estimating directivity and gain of antennas," in IEEE Antennas and Propagation Magazine, vol. 40, no. 4, pp. 7-11, Aug. 1998.
30. I. Donevski, J.J. Nielsen, "Dynamic Standalone Drone-mounted Small Cells" 2020 European Conference on Networks and Communications (EuCNC), Dubrovnik, Croatia, 2020.

This document reflects only the author's view and the Agency is not responsible for any use that may be made of the information it contains.